PHYSICAL REVIEW B VOLUME 32, NUMBER 10 15 NOVEMBER 1985

Self-consistent calculations of rare-gas—transition-metal interaction potentials

D. Drakova,* G. Doyen, and F. v. Trentini
Institut für Physikalische Chemie, Ludwig-Maximilians-Universität München, D-8000 München 2, Theresienstrasse 37, Federal Republic of Germany
(Received 26 February 1985)

A model Hamiltonian is used to calculate potential-energy surfaces for He and Ne on the (110) faces of Ni, Cu, Pd, and Ag. The calculations are nonperturbative, self-consistent, and contain no parameters which are fittable with respect to the gas-solid interaction. Static image-force effects are included. The theory represents the first quantum-mechanical approach to rare-gas—transition-metal potentials which includes the interaction of the rare-gas orbitals with the *d* electrons in a consistent way. Corrugation is found to be approximately proportional to the *d*-electron charge density. The *sp* band is represented by a Sommerfeld model with hybridization gap, which does not contribute to the corrugation. Part of the potential arises through the hybridization of the rare-gas orbitals with the unoccupied metal states. This interference energy is roughly a factor of 2 larger for neon than for helium, leading to larger corrugations of the neon potentials as compared with the helium potentials. This is in agreement with recent experiments, but in contrast to earlier theoretical predictions. The theoretically calculated corrugations and well depths compare reasonably to the experimental data where available. The computed values of corrugation for He increase in the order Ni, Cu, Ag, and Pd. This agrees with experiments where soft potentials have been fitted to the scattering data, although the predicted He/Ni(110) corrugation is overly large by more than a factor of 2. With increasing energy, the He corrugation increases slightly in the calculations. The dependence is nearly constant for Ni and strongest for Pd. For Ne/Ni(110) and Ne/Pd(110) corrugation decreases with energy. Image-force effects are found to be important for the corrugation and softness of the neon potentials.

I. INTRODUCTION

Recent advancements in experimental techniques (improved intensity and experimental resolution) led to the observation of helium diffraction from a number of transition-metal surfaces: W(112),[1] Cu(100),[2] Cu(117),[3] Cu(110),[4] Cu(113),[4] Cu(115),[4] Ni(110),[5] Ag(111),[6] Ag(110),[7] Pd(110),[8] and the reconstructed Au(110) surface.[9] For the smooth fcc (111) and (100) surfaces the nonspecular intensities are so weak that no meaningful information about the He-metal interaction potential can be obtained. For the open (113), (115), and (117) structures the shape is so complicated and the corrugation amplitudes are so large that most methods for calculating diffraction intensities either stop working or become prohibitively complicated. The bound-state resonances are, however, easily observable for these strongly corrugated surfaces and the well depths and energy levels have been determined.[3,4]

The fcc (110) faces present an intermediate situation in that the corrugation amplitude is usually large enough for being analyzed by the standard methods, but it is too small for the bound-state resonances to be observable.[10] An exception is Ag(110), which shows an unexpectedly large corrugation so that selective adsorption data are available.[7] These favorite circumstances permitted the construction of an "experimental He/Ag(100) interaction potential." If one combines the information about the adsorption well obtained from the He/Cu(113) and He/Cu(115) data with the He/Cu(110) diffraction intensities, one can derive what with some justifications might be termed an experimental He/Cu(110) interaction potential.[11,12]

These experimental interaction potentials offer an ideal testing ground for adsorption theories. Quite a few schemes have been developed in order to predict the interaction energies of rare gases with metal surfaces. Many of them[13–16] pay special attention to the so-called "van der Waals force," which is taken as the only attractive contribution. The repulsive part of the interaction is estimated *independently* by either using the Hartree-Fock approximation[13] or the density-functional formalism.[15,16] The superposition of the attractive and repulsive forces produces then a minimum. This separation of the total interaction energy is inadequate, because somewhere near the equilibrium distance the van der Waals interaction loses its clear-cut character and merges into the exchange-correlation interaction which has the same physical origin as the repulsive interaction. Therefore both contributions should be determined together in a coherent fashion by solving Schrödinger's equation. This point has already been emphasized in the literature.[17–19]

Recently, Annett and Haydock[20] pointed out that the hybridization of the 1*s* orbital with the unoccupied metal states yields an important contribution to the attractive interaction energy, which has been neglected in the above-mentioned approaches.

The local-density formalism provides an adequate approach for *s*-band metals.[18] Treatment of the corrugation on transition-metal surface due to interaction with the *d*

 ©1985 The American Physical Society

electrons is much more difficult in this formalism and no calculations are available yet. A remedy is commonly sought by applying the Esbjerg-Nørskov assumption,[21] which states the proportionality between surface charge density and helium potential energy. The validity of this assumption is presently under controversial discussion.[11,19]

Employing the Esbjerg-Nørskov assumption together with the proportionality factors calculated by Puska, Nieminen, and Maninnen[22] leads to the conclusion that the corrugation determined from neon scattering should be smaller than that determined from helium scattering. The experimental results obtained by Rieder and Stocker[8] and Salanon[23] demonstrate the opposite behavior.

The present paper calculates helium and neon interaction potentials by obtaining the Hartree-Fock solution of a model Hamiltonian, which has already been applied successfully to reactive chemisorption systems (H,O, CO, and NO on the same transition metals as investigated here).[24]

The structure of the paper is as follows. Section II describes the model Hamiltonian. Only those terms which are relevant for the rather weak rare-gas—metal interaction are discussed. Section III explains the parametrization and Sec. IV comments briefly on technical details of the numerical procedure. The calculated potential-energy surfaces are presented in Sec. V. Section VI contains the physical discussion of the results.

II. THE MODEL

The model has been described previously.[25] It has been used successfully to explain and correlate experimental data over a wide class of chemisorption systems.[24] The same computer program is used here to calculate the physisorption of rare-gas atoms. Because of the repulsive character of the interaction, the classical turning point for thermal kinetic energies is at large distances, where the overlap is rather small. Interaction terms which are of higher than second order in the overlap are therefore of little importance and need not be considered in order to elucidate the physical picture. The relevant terms in the Hamiltonian are then

$$H = H_0 + H_1 + H_2 + H_3 + \cdots , \tag{1a}$$

$$H_0 = \sum_A E_A^0(\tilde{n}_{A\uparrow}+\tilde{n}_{A\downarrow}) + \sum_k \varepsilon_k(\tilde{n}_{k\uparrow}+\tilde{n}_{k\downarrow}) + \sum_{A,B}(AA\mid BB)(\tilde{n}_{A\uparrow}\tilde{n}_{B\downarrow}+\tilde{n}_{A\downarrow}\tilde{n}_{B\uparrow}) + \sum_{\substack{A,B\\A\neq B}}[(AA\mid BB)-(AB\mid BA)](\tilde{n}_{A\uparrow}\tilde{n}_{B\uparrow}+\tilde{n}_{A\downarrow}\tilde{n}_{B\downarrow}) , \tag{1b}$$

$$H_1 = -\sum_{A,B}^{\text{occupied}}\sum_{k,l}[2(BB\mid AA)-(AB\mid BA)]\langle A\mid l\rangle\langle k\mid A\rangle(\tilde{a}^\dagger_{k\uparrow}\tilde{a}_{l\uparrow}+\tilde{a}^\dagger_{k\downarrow}\tilde{a}_{l\downarrow}) + \tfrac{1}{2}\sum_{\substack{A,k\\s=\uparrow,\downarrow}}\left[\left[E_A^0+\varepsilon_k+\sum_B(BB\mid AA)\tilde{n}_{B-s}+\sum_{B(\neq A)}[(BB\mid AA)-(AB\mid AB)]\tilde{n}_{Bs}\right]\times(\langle A\mid k\rangle\tilde{a}^\dagger_{As}\tilde{a}_{ks}+\langle k\mid A\rangle\tilde{a}^\dagger_{ks}\tilde{a}_{As})\right] + \sum_{\substack{A,k,l\\s=\uparrow,\downarrow}}\left[\left[\sum_B(BB\mid AA)\tilde{n}_{B-s}+\sum_{B(\neq A)}[(BB\mid AA)-(AB\mid BA)]\tilde{n}_{Bs}\right]\langle A\mid l\rangle\langle k\mid A\rangle\tilde{a}^\dagger_{ks}\tilde{a}_{ls}\right] , \tag{1c}$$

$$H_2 = 2\sum_{A,B,k}^{\text{occupied}}[2(BB\mid AA)-(AB\mid BA)]\,|\langle A\mid k\rangle|^2 + V_{\text{dipole}}(\mathbf{r}_0) , \tag{1d}$$

$$H_3 = -Q^2V_{im}(z) , \tag{1e}$$

where the ellipsis represents unspecified terms of higher order in the overlap.

The indices A and B refer to the rare-gas-atom basis orbitals; the indices k and l label unperturbed transition-metal states; $\tilde{a}_i$, $\tilde{a}_i^\dagger$, and $\tilde{n}_i$ are the electron destruction, creation, and number operators, respectively. The tilde on these operators indicates that the wave functions are not mutually orthogonal. $\langle A\mid k\rangle$ is the common Dirac notation for the overlap, which in the notation of Eq. (1) is assumed to be independent of the spin orientation. E_A^0 is an "effective" core attraction integral on the gas atom; $(AA\mid BB)$ and $(AB\mid BA)$ are effective gas-atom Coulomb and exchange integrals, respectively. The meaning and parametrization of these quantities is discussed in Sec. III. The physically interesting aspect of the Hamiltonian is that electron-electron repulsion is included explicitly and consistently in the local region overlapped by the gas-atom wave functions. This leads to a "dynamic" (i.e., occupancy dependent) electron hopping between the metal surface and the gas atom (second term of H_1 of the Hamiltonian).

H_0 describes the separated system, i.e., the gas atom and metal surface without interaction H_1 contains the electronic interaction. H_3 represents the attractive image

potential of the gas-atom core of charge Q. The higher-order terms not written down in Eq. (1) are retained in the numerical calculations but are not discussed here. H_2 describes the repulsion between the positive-ion cores. This term has not been included in the earlier calculations,[24] and therefore we present a detailed motivation for it in the following.

The Hamiltonian assumes partial cancellation of large electrostatic terms:

$$2\sum_{A}^{\text{occupied}}\langle A\,|\,V^{\dagger}_{\text{metal}}(\mathbf{r})\,|\,A\rangle+2\sum_{A,k}^{\text{occupied}}[2(AA\,|\,kk)-(Ak\,|\,kA)]=2\sum_{A,k}^{\text{occupied occupied}}\sum_{B}[2(BB\,|\,AA)-(AB\,|\,BA)]\,|\,\langle A\,|\,k\rangle\,|^2\,. \tag{2}$$

The sums run only over occupied electron states. The factor 2 accounts for spin degeneracy, assuming a closed-shell system. Of the total electron-electron repulsion between the gas atom and the metal only the right-hand side of Eq. (2) is retained in the Hamiltonian (cf. H_1), i.e., only that part of the repulsion which is not canceled by a corresponding attraction $V^{\dagger}_{\text{metal}}$ of the metal-ion cores.

A detailed discussion of the motivation for Eq. (2) can be found in Ref. 25 and is not repeated here. The described choice of the electron-electron repulsion implies that the adelectron—metal-ion attraction is completely compensated by a part of the electron-electron repulsion:

$$\sum_{A}^{\text{occupied}}\langle A\,|\,V^{\dagger}_{\text{metal}}(\mathbf{r})\,|\,A\rangle=-U=\sum_{A,k}^{\text{occupied}}\left[\sum_{B}^{\text{occupied}}[2(BB\,|\,AA)-(AB\,|\,BA)]\,|\,\langle A\,|\,k\rangle\,|^2-2[(AA\,|\,kk)-(Ak\,|\,kA)]\right]. \tag{3}$$

Perfect cancellation is also assumed between the attraction of the metal electrons by the gas-atom core and the discussed gas-atom—metal electron—electron repulsion (cf. Ref. 25):

$$2\sum_{k}^{\text{occupied}}\langle k\,|\,(-Q/|\,\mathbf{r}-\mathbf{r}_0\,|\,)\,|\,k\rangle+2\sum_{A,k}^{\text{occupied}}[2(AA\,|\,kk)-(Ak\,|\,kA)]=0\,, \tag{4}$$

where $\mathbf{r}_0$ is the position of the gas-atom core. The left-hand side of this equation is called penetration integral. Using this relationship as an approximation for the metal-electron—gas-atom core attraction means introducing a Goeppert-Mayer—Sklar potential (GMS) (first term in H_1).

If we consider the positive charge Q of the gas-atom core in the field of the unperturbed metal surface, we have the following exact relationship:

$$\sum_{M}Q/|\,\mathbf{r}_0-\mathbf{r}_M\,|+2\sum_{k}^{\text{occupied}}\langle k\,|\,-Q/|\,\mathbf{r}-\mathbf{r}_0|\;|\,k\rangle=V_{\text{dipole}}(\mathbf{r}_0)\,, \tag{5}$$

where $\mathbf{r}_M$ denotes the position of a metal-ion core. Using Eqs. (3) and (4) and defining

$$\sum_{M}Q/|\,\mathbf{r}_0-\mathbf{r}_M\,|=2U+E^{\text{rep}}\,,$$

we obtain the following expression for the effective repulsion;

$$E^{\text{rep}}=V_{\text{dipole}}(\mathbf{r}_0)+2\sum_{k,A,B}^{\text{occupied}}[2(BB\,|\,AA)-(AB\,|\,BA)]\times|\,\langle A\,|\,k\rangle\,|^2\,. \tag{6}$$

This core-core repulsion is contained in H_2. It had not been included in previous calculations based on the same electronic model Hamiltonian, but it has been demonstrated here that this form of the core-core repulsion follows in a logical way from the structure of the electronic Hamiltonian. The handling of the electrostatic interaction between adsorbate and metal can hence be summarized as follows. There are four electrostatic terms:

$$W(\text{adsorbate electrons—metal cores})=-2U\,,$$

$$W(\text{adsorbate core—metal electrons})=-2U-2\Delta U\,,$$

$$W(\text{adsorbate core—metal cores})=V_{\text{dipole}}+2U+2\Delta U\,,$$

$$W(\text{adsorbate electrons—metal electrons})=2U+2\Delta U\,.$$

Here ΔU and U are defined by Eqs. (2) and (3), respectively. The factor 2 arises from spin degeneracy.

All four terms contain the quantity $2U$. In the model Hamiltonian the electrostatic terms are therefore "renormalized" by reducing the absolute magnitude of all four terms by $2U$. In this way the electrostatic balance is preserved.

III. PARAMETRIZATION

The parametrization consists of choosing the wave functions and the one- and two-electron integrals in such a way that the description of the *separated* system (no interaction between gas atom and metal surface) agrees with available experimental data. An effective one-electron description is used, which for the gas atom contains electron-electron integrals explicitly, whereas for the metal an independent-particle model is the starting point. Fitting a one-electron picture to experimental data means including correlation effects implicitly. This is essential, because a Hartree-Fock (HF) description of the separated system is inadequate. A HF treatment of the metal would, e.g., lead to a spurious density of states at the Fermi level.[26]

TABLE I. Core energy E_{1s} and Coulomb integral $(1s\,1s \mid 1s\,1s)$ of the helium $1s$ function. Correction z_{A0}^{He} to the position of the image plane for the helium calculations.

$E_{1s}=-54.44$ eV
$(1s\,1s \mid 1s\,1s)=29.88$ eV
$z_{A0}^{He}=1.36$ a.u.

A. Rare-gas-atom description

The gas-atom orbitals are Slater-type orbitals (STO's) with the exponents taken from Clementi's tables.[27] The orbitals are identical for different spin orientations. For helium only the $1s$ orbital is included. For neon the $1s$ orbital is considered to be nonpolarizable and therefore forms a part of the effective core of charge $+8e$. The $2s$ and $2p$ orbitals are explicitly treated in the calculations. The core energies E_A^0 and the Coulomb and exchange integrals $(AA \mid BB)$ and $(AB \mid BA)$ are reproduced in Tables I and II. They are not evaluated by direct integration but are chosen in such a way that the experimental spectroscopic data are reproduced. For helium, e.g., this warrants that the total energies of the $(1s^2)$ $(1s,2s)$, and $(1s,2s)$ configurations and their ionization energies agree with experiment.

B. Description of the metal surface

The inner potential of the delocalized electrons of the sp band is approximated by a step function (Sommerfeld model). Inside the metal the electrons are attracted by a potential V_0 which is given by the sum of the work function ϕ and the energetic width E_F of the filled sp band. Outside the metal the potential is zero. With z defined as the perpendicular distance from the step the potential is given by Eq. (7):

$$V(z')=\begin{cases}V_0, & z'<0 \text{ with } V_0=-\phi-E_F\ , \\ 0, & z'>0\ .\end{cases} \tag{7}$$

The eigenfunctions of this potential are sines, which decay exponentially in front of the surface:

$$\psi_{sp\ \text{band}}(z')=\begin{cases}A\sin[(k_z z'+\alpha)], & z'<0 \\ (Ak_z/K)\exp[-(K^2-k_z^2)^{-1/2}z'], & z'>0\end{cases}$$
$$A=(2/L)^{1/2},\quad K^2/2=E_F+\phi\ , \tag{8}$$
$$\alpha=\arctan[-k_z(K^2-k_z^2)^{-1/2}]\ .$$

TABLE II. Core energies E_A, Coulomb integrals $(AA \mid BB)$, and exchange integrals $(AB \mid BA)$ for the neon $2s$ and $2p$ functions $(A,B=2s,2p;\ a,b=x,y,z)$. Correction z_{A0}^{Ne} to the position of the image plane.

$E_{2s}=-112.47$ eV
$E_{2p}=-87.56$ eV
$(2s\,2s \mid 2s\,2s)=(2s\,2s \mid 2p\,2p)=(2p\,2p \mid 2p\,2p)=10.00$ eV
$(2s\,2p \mid 2p\,2s)=2.00$ eV
$(2p_a 2p_b \mid 2p_b 2p_a)=1.00$ eV
$z_{A0}^{Ne}=0.68$ a.u.

The normalization length L is assumed to be so large that for normalizing the wave function the exponential decaying parts can be neglected. Parallel to the surface (x,y coordinates) periodic boundary conditions are used:

$$\Psi_{sp\ \text{band}}=L^{-1/2}\psi_{sp\ \text{band}}(z')\exp[i(k_x x+k_y y)]\ , \tag{9}$$

where k_x and k_y are the wave vectors in x and y direction, respectively. The density of states in $\mathbf{k}$ space is $L^3/4\pi^3$.

The d orbitals are approximated by double-ζ functions centered at the different lattice sites. As the sp electrons are delocalized throughout the crystal, the atomic wave functions of the corresponding positive ions (with the same d configuration as in the metal) are used. The exponents and coefficients are shown in Table III. As the metals under consideration have narrow d bands the effective density of d states is approximated by a δ function in energy. In order to determine the dipole potential of the unperturbed metal surface, the total electronic charge has to be calculated. The d states are strongly localized, however, and do not contribute significantly to the "spill-over" of the metal electrons, and hence can be neglected for the dipole potential. The effective part $n_-(z')$ of the electronic charge is given by the integral over the absolute squares of the sp wave functions [Eq. (9)] up to the Fermi level. In order to obtain charge neutrality a positive uniform jellium of density n_+ is introduced. Inside the metal ($z'\to-\infty$) both charge densities cancel each other:

$$\lim_{z'\to-\infty} n_+(z')=-\lim_{z'\to-\infty} n_-(z')=n_0\ .$$

The positive charge density $n_+(z')$ of the jellium has a step at the distance $-R_{JS}$ relative to the Sommerfeld edge:

$$n_+(z)=\begin{cases}n_0, & z'<-R_{JS} \\ 0, & z'>-R_{JS}\ .\end{cases} \tag{10}$$

The distance R_{JS} is determined by the overall charge neutrality of the metal:

$$\int [n_+(z')+n_-(z')]dz'=0\ . \tag{11}$$

The dipole potential is given by

$$V_{\text{dipole}}(z')=2\pi\int [n_+(z)+n_-(z)]\,|z'-z|\,dz\ . \tag{12}$$

The first layer of lattice sites is situated relative to the jellium edge ($-R_{JS}$) at $d/2$, where d is the distance to the next layer inside the metal. This choice is somewhat arbitrary, but it is the standard procedure in the literature. All relevant distances are shown in Fig. 1.

Due to the interaction of the sp band with d bands of the same symmetry a hybridization gap is formed.[29–31] In the model this behavior is introduced by omitting the sp states of a certain energy interval $(\varepsilon_1,\varepsilon_2)$. These energies (with respect to the vacuum level) together with work functions, Fermi energies, the distance R_{JS} as well as the lattice constants are compiled for all relevant metals in Table IV.

TABLE III. Orbital exponents ζ_i and coefficients c_i used in the expansion of nd metal wave functions Ψ_d in Slater basis wave functions ψ_{nlm}. Only components with exponents $\zeta_i < 6$ are displayed. Components which larger exponents give negligible overlap with the adorbitals, but are essential for normalization. The d wave functions have the form

$$\psi_d = \sum_i c_i \psi_{nlm}(r;\zeta_i), \quad \psi_{nlm}(r;\zeta_i) = [(2\zeta_i)^{2n+1}/(2n)!]^{1/2} r^{n-1} \exp(-\zeta_i r) Y_{lm}(\theta,\phi) .$$

Metal	Quantum numbers n	l	ζ_i	c_i	Ref.
Cu	3	2	2.30	0.5744	33(a)
	3	2	5.95	0.5933	
Ni	3	2	1.570 27	0.210 53	33(b)
	3	2	2.787 09	0.417 73	
	3	2	4.752 53	0.331 29	
Pd	4	2	2.398	0.6405	33(c)
	4	2	5.542	0.5823	
Ag	4	2	2.444	0.5809	33(d)
	4	2	4.908	0.5833	

C. Image potential

The model Hamiltonian as described in Sec. II contains a correlated electron motion only in the region overlapped by the adorbitals. In the presence of a metal surface the image force is an important nonlocal correlation effect which even for rare-gas atoms leads to relatively large shifts of the ionization energies (of the order of several eV). This has been experimentally confirmed by means of the ion neutralization spectroscopy.[34] In the present version of our model image-force effects are included in a static way as renormalizing the core and Coulomb integrals.

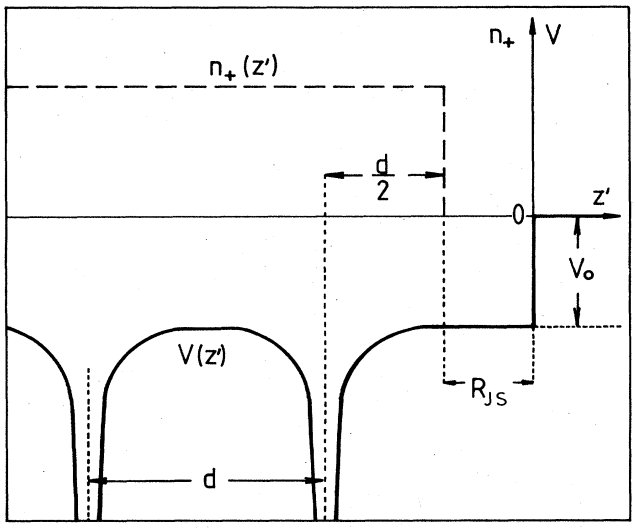

FIG. 1. Definition of various surface planes (plane of lattice sites, jellium edge, Sommerfeld edge) and their relative distances. Perpendicular distances z are given in this paper relative to the first plane of lattice sites, positive distances correspond to the vacuum side ($z = \tilde{z} + d/2 = z' + R_{JS} + d/2$).

Consider the effect of all image charges of the rare-gas charge distribution on one particular rare-gas electron. The interaction of the electron with its own image leads to an attractive potential $-V_{\rm im} = -1/(4\,|\,z'-z_{\rm im}\,|\,)$. $z_{\rm im}$ is the position of the image plane, which will be discussed later. z' is the (averaged) position of the considered electron. The interaction energy of the electron with the image of the core of charge Q is $Q/(2\,|\,z'-z_{\rm im}\,|\,)$. Here we have assumed that the averaged position of the rare-gas electron is right at the position of the core. This interaction energy is different in magnitude from $V_{\rm im}$, because the image of the core does not move, if the considered electron moves. The same is true for the images of the $(Q-1)$ other electrons on the rare-gas atom. Hence the total interaction energy of all images with the considered electron is

$$-1/(4\,|\,z'-z_{\rm im}\,|\,)+Q/(2\,|\,z'-z_{\rm im}\,|\,) -(Q-1)/(2\,|\,z'-z_{\rm im}\,|\,)=1/(4\,|\,z'-z_{\rm im}\,|\,)=V_{\rm im}(z') .$$

We want to describe this by a renormalization of the gas-atom parameters:

$$E_A^0(z)=E_A^0(\infty)+\Delta E_A(z') ,$$
$$(AA\,|\,BB)\,|_{z'}=(AA\,|\,BB)\,|_{z'=\infty}-\Delta W(z') , \qquad (13)$$
$$(AB\,|\,BA)\,|_{z'}=(AB\,|\,BA)\,|_{z'=\infty} .$$

This leads to

$$V_{\rm im}(z')=\Delta E_A(z')-(Q-1)\Delta W(z') .$$

On the other hand, the total gas-atom energy has to remain unchanged, because a neutral gas atom experiences no net image force:

$$Q\Delta E_A(z')-\tfrac{1}{2}Q(Q-1)\Delta W(z')-Q^2V_{\rm im}(z')=0 . \qquad (14)$$

The last two equations can be solved for $\Delta E_A(z)$ and $\Delta W(z)$:

TABLE IV. Parametrization of the metal surface: ϕ, work function (eV); E_F, Fermi energy (eV); ε_1, upper edge of hybridization gap relative to Fermi level (eV); ε_2, lower edge of hybridization gap relative to Fermi level (eV); a, lattice constant (a.u.); d, distance between (110) metal layers in the z direction (a.u.); R_{JS}, separation between jellium edge and Sommerfeld edge (a.u.); B, constant for the $T-B$ method (see text).

Metal	ϕ (eV)	Ref.	E_F (eV)	ε_1 (eV)	ε_2 (eV)	Ref.	a (a.u.)	d (a.u.)	R_{JS} (a.u.)	B
Cu	4.50	28	9.35	−7.38	−9.43	29	6.8340	2.4162	0.3404	0.85
Ni	5.04	28	9.00	−6.76	−9.62	29	6.6636	2.3560	0.3799	0.70
Pd	5.40	28	7.00	−7.44	−9.92	30	7.3528	2.5996	0.5232	0.88
Ag	4.52	28	8.89	−10.07	−12.07	31	7.7244	2.7310	0.3614	0.91

$$E_A(z')=V_{\rm im}(z')(2Q-1)\ ,$$
$$\Delta W(z')=2V_{\rm im}(z')\ . \tag{15}$$

If the Q values for helium ($Q=2$) and neon ($Q=8$) are inserted, one finds

$$\Delta E_A^{\rm He}(z')=3V_{\rm im}(z'),\ \Delta E_A^{\rm Ne}(z')=15V_{\rm im}(z')\ . \tag{16}$$

This parametrization has the property that it yields the right image interaction also for the ionized configurations. Assume there is the charge q on the gas atom. The change of the total energy due to image-force effects is then

$$\begin{aligned}&(Q+q)\Delta E_A-(Q+q)(Q+q-1)\Delta W/2-Q^2V_{\rm im}\\&=[(Q+q)(2Q-1)-(Q+q)(Q+q-1)-Q^2]V_{\rm im}\\&=-q^2V_{\rm im}\ .\end{aligned}$$

The gas-atom parameters E_A^0 and $(AA\,|\,BB)$ of the Hamiltonian [Eq. (1)] are the distance dependent quantities defined in Eq. (13). This distance dependence decreases the total energy of the system as the gas atom approaches the surface. But according to Eq. (14) this decrease is canceled exactly by the gain in energy due to the interaction of the gas core with its image. Because the renormalized quantities E_A^0 and $(AA\,|\,BB)$ enter in the interaction terms H_1 of the Hamiltonian [Eq. (1)], the image force influences also the hybridization of wave functions.

Appelbaum and Hamann[35] calculated the image potential $V_{\rm im}(\tilde{z})$ of a static point charge Q near a metal surface. The surface was treated in the jellium approximation and the response of the semi-infinite electron gas was calculated self-consistently in the local-density formalism. For not too small distance $\tilde{z}$ of the charge from the jellium edge the image potential could be approximated by

$$V_{\rm im}=Q^2/[4\,|\,\tilde{z}-r_{\rm im}(\tilde{z})\,|\,]\ , \tag{17}$$

where $r_{\rm im}$ depends on the distance $\tilde{z}$ as well. In Fig. 2 this dependence is shown for different electron densities $-n_0$, given by the Wigner-Seitz radius r_s:

$$n_0=3/4\pi r_s^3\ . \tag{18}$$

The functions $r_{\rm im}(\tilde{z})$ are approximated by two linear functions in this work (dashed lines in Fig. 2):

$$r_{\rm im}(\tilde{z})=\begin{cases}1.36-0.18r_s, & \tilde{z}>A(r_s)\\ [(1.76-0.18r_s)/(1.40+0.30r_s)]\tilde{z}-0.40, & \tilde{z}<A(r_s)\end{cases}$$
$$A(r_s)=1.40+0.30r_s\ ,$$
$$z_{\rm im}=r_{\rm im}-R_{\rm JS}\ . \tag{19}$$

The arguments given up to now are valid for point charges, whereas in reality we have smeared out electron charge distributions. If the image force is averaged properly over these distributions, the effective electron position would not coincide with the position of the core. To account for this we make a correction to $z_{\rm im}$:

$$z_{\rm im}^A=z_{\rm im}+r_{A0}^A\ . \tag{20}$$

The values used in the calculations are

$$r_{A0}^{\rm He}=1.36\ \text{a.u.},\ r_{A0}^{\rm Ne}=0.68\ \text{a.u.},\ r_s=2.2\ \text{a.u.}\ .$$

The corrected $z_{\rm im}$ value is used for both, the images of the electrons and the image of the core. If one would apply it only to the electrons, a long-range attractive potential for the neutral gas atoms would result. This long-range at-

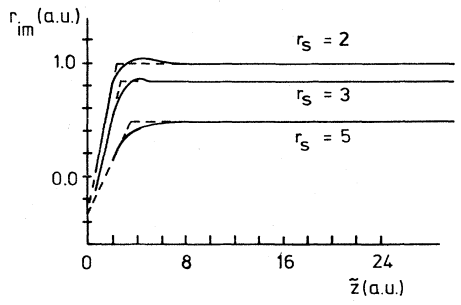

FIG. 2. Position of the image plane according to Appelbaum and Hamann (Ref. 35). The dashed curves are the values used in the present work. The ordinate gives the position relative to the jellium edge.

traction would, however, not be a correct representation of the van der Waals potential. The described procedure of estimating image effects is in the case of helium used for all distances. In the case of neon some care is needed, however. If Eqs. (15), (17), and (19) are applied at close distances or inside the positive jellium, it might happen that the two-electron integrals Eq. (13) will become very small or even negative. This happens, in fact, for neon, because the asymptotic electron-electron integrals are significantly smaller than for helium (~ 10 eV compared to 30 eV). We therefore stop varying $V_{\rm im}$, once $(AA\,|\,BB)-(AB\,|\,AB)$ becomes smaller than ~ 2.5 eV. For neon this occurs roughly 4 a.u. in front of the first atomic layer.

IV. DISCRETIZATION AND OVERLAP INTEGRALS

The Hamiltonian is diagonalized numerically on a computer. This is possible if the continuous metal spectrum is discretized. The method has been described in detail.[36] Essentially the same discretization is used as in previous calculations. The d band is represented by a single discretized band, which is considered to be occupied for all four metals. The sp band is split up into six discretized subbands. For the Pd calculations one subband is intersected by the Fermi level although it is considered to be fully occupied. This introduced a certain error. Some test calculations lead to the conclusion that the error introduced by the rather coarse discretization on, e.g., the corrugation is $\sim 20\%$. This error can be reduced considerably by using a much finer discretization. The numerical expense, however, does not appear to be justified in view of other uncertainties in the model. The data characterizing the employed discretization is summarized in Fig. 3.

The overlap integrals are evaluated by explicitly constructing the "adsorbate-projected metal states" $|\,k\lambda A\,\rangle$ (k symbolizes the metal character and λ labels the subband):

$$|\,k\lambda A\,\rangle = \frac{1}{|\,\langle A\,|\,k\lambda A\,\rangle\,|}\sum_{l\in\lambda}\langle l\,|\,A\,\rangle\,|\,l\,\rangle\ . \tag{21}$$

For the sp band $|\,l\,\rangle$ represents a Sommerfeld wave function as described in Sec. III. For the d band the situation is more complicated and the reader is referred to the discussion in Ref. 36. The "$T-B$ method" described there has been used in the present work. The values of the parameter B are listed in Table IV. They have been obtained by fitting the $T-B$ method for an on-top potential-energy curve to the "first principles" results obtained with the assumption that the atomic d orbitals on different centers are mutually orthogonal. This first principles method has been found to overestimate corrugation,[25] and therefore the $T-B$ method is to be preferred. In contrast to earlier chemisorption calculations,[24] B is not obtained by a fit to experiment. Instead it is calculated within the framework of the theory based on the idea that the assumption of mutual orthogonal d orbitals cannot lead to a large error, if the adsorbate overlap with a single particular center dominates. This is the case for the on-top position.

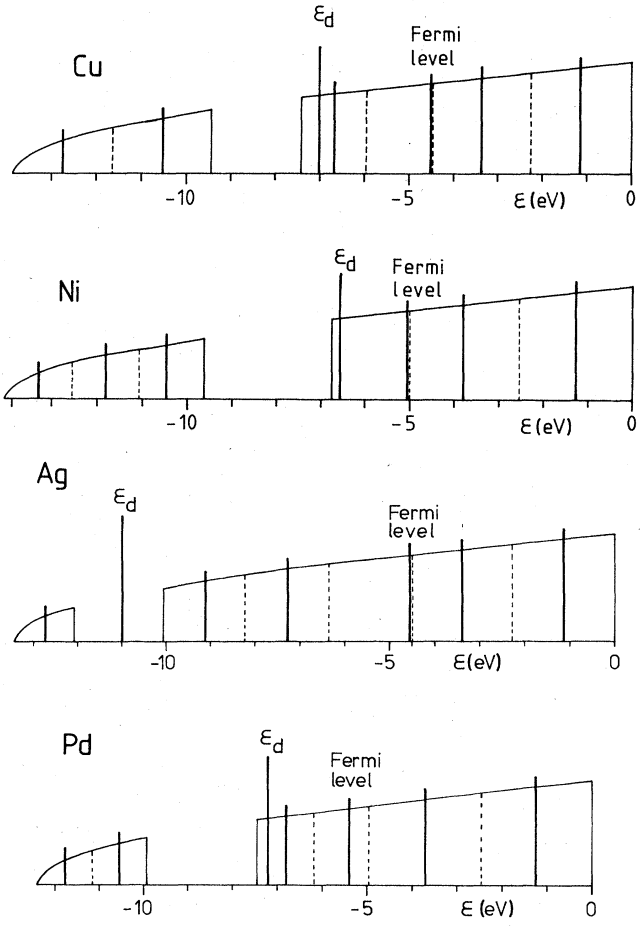

FIG. 3. Density of states, hybridization gap, and discretization used for the numerical calculations. The solid vertical bars correspond to the discretized subbands, the dashed lines indicate the energy intervals which they represent. Energy zero corresponds to the vacuum level. For the neon calculations each subband is fourfold degenerate, i.e., there are four different adsorbate projected metal states per discretized level.

The B values obtained in this way are considerably larger than those obtained previously by a fit to experiment.[24] The reason is that in the older calculations the core repulsion energy $E^{\rm rep}$ (cf. Sec. II) has not been included. The smaller B values accounted for this by reducing the gain in electronic energy. Including $E^{\rm rep}$ explicitly, the "theoretically" determined B values lead to reasonable agreement with experiment, as will be demonstrated in the following sections.

The overlap integrals are evaluated numerically on a computer. For the d overlap three layers are included. Overall, 300 lattice sites are summed, assuring complete convergence of the overlaps.

V. RESULTS

A. Potential-energy curves for special lateral geometries

Figures 5–9 show the calculated potential-energy curves perpendicular to the surface for the four high-symmetry geometries (cf. Fig. 4): (i) in the center between

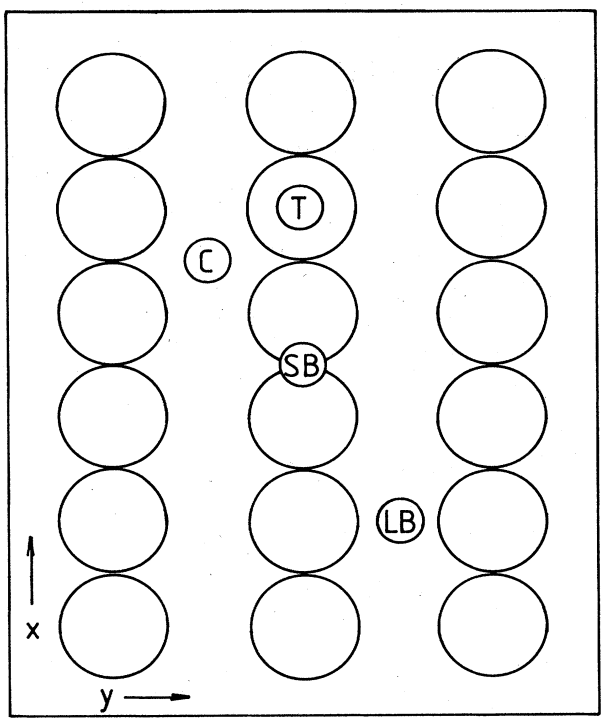

FIG. 4. High-symmetry geometries for the (110) fcc face: SB, short-bridge position; LB, long-bridge position; C, position in the center of the unit cell; and T, position on top of a metal atom.

four metal atoms (C); (ii) in the center of the short bridge in the close-packed direction (SB); (iii) in the center of the long bridge (LB); (iv) on top of a metal atom (T).

Harris and Liebsch[11] fitted an analytically derived potential shape to experimental He/Cu(110) diffraction data by Perreau and Lapujoulade[4] and managed to get quantitative agreement. (The "experimental" potential obtained by Garcia, Barker, and Batra[12] essentially agrees with that of Harris and Liebsch.) This potential has only a one-dimensional corrugation (in the less-close-packed [100] direction). We recalculated the Harris-Liebsch potential as a function of perpendicular distance for the points of extremal corrugation and compare it in Fig. 6 to our model Hamiltonian results for center and short bridge. The absolute distance from the physical surface (plane of metal ion cores) cannot be determined experimentally. We therefore shifted the Harris-Liebsch distance scale. In general the Harris-Liebsch fit compares reasonably to our calculations. The main differences are the missing long-range van der Waals tail in the model Hamiltonian approach (cf. Sec. VI) and a steeper increase of the repulsive part of our potential.

A similar fit to He/Ag(110) selective adsorption resonances and all available diffractive scattering data was performed by Schinke and Luntz,[7] and a comparison with the model Hamiltonian results is presented in Fig. 8. The repulsive part of the theoretical potential turns out to be steeper than the fitted curve from Schinke and Luntz. Garcia, Barker, and Rieder[37] fitted a soft potential with van der Waals minimum to the He/Ni(110) scattering data. In Fig. 7 this potential is compared to our theoretical results.

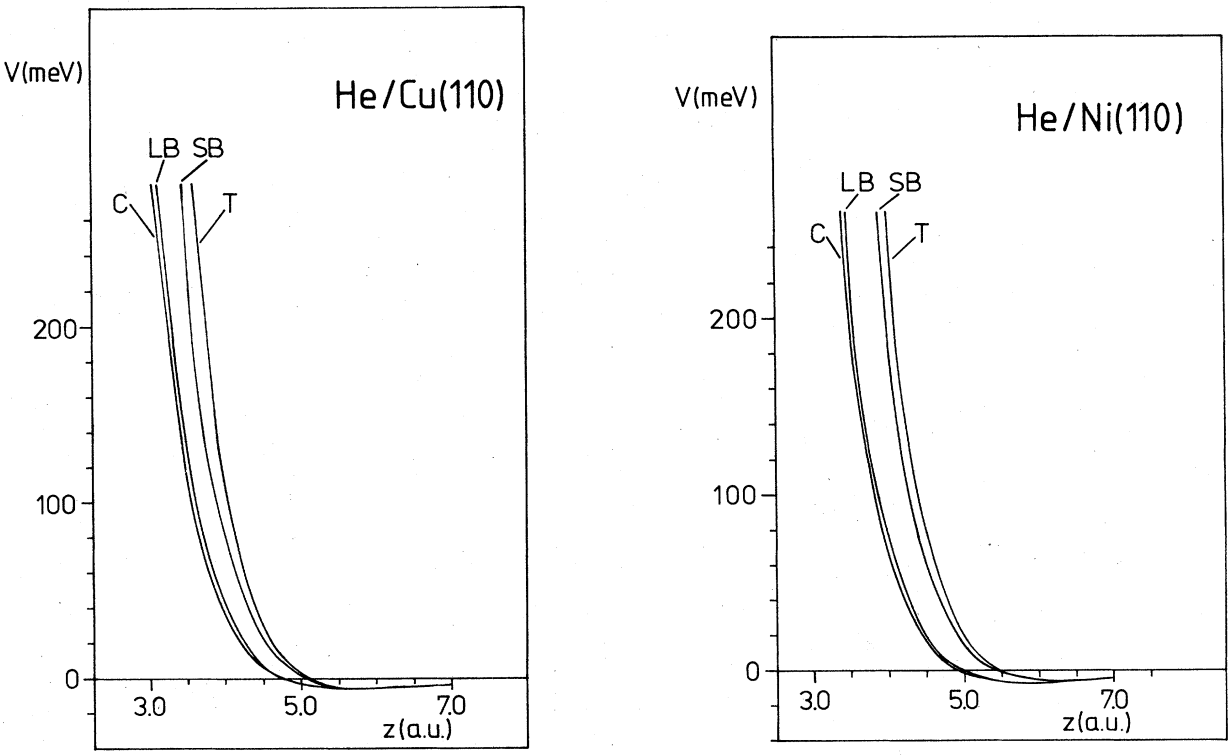

FIG. 5. Calculated potential energy curves perpendicular to the (110) surfaces for adsorption of He above the four high-symmetry positions indicated in Fig. 4.

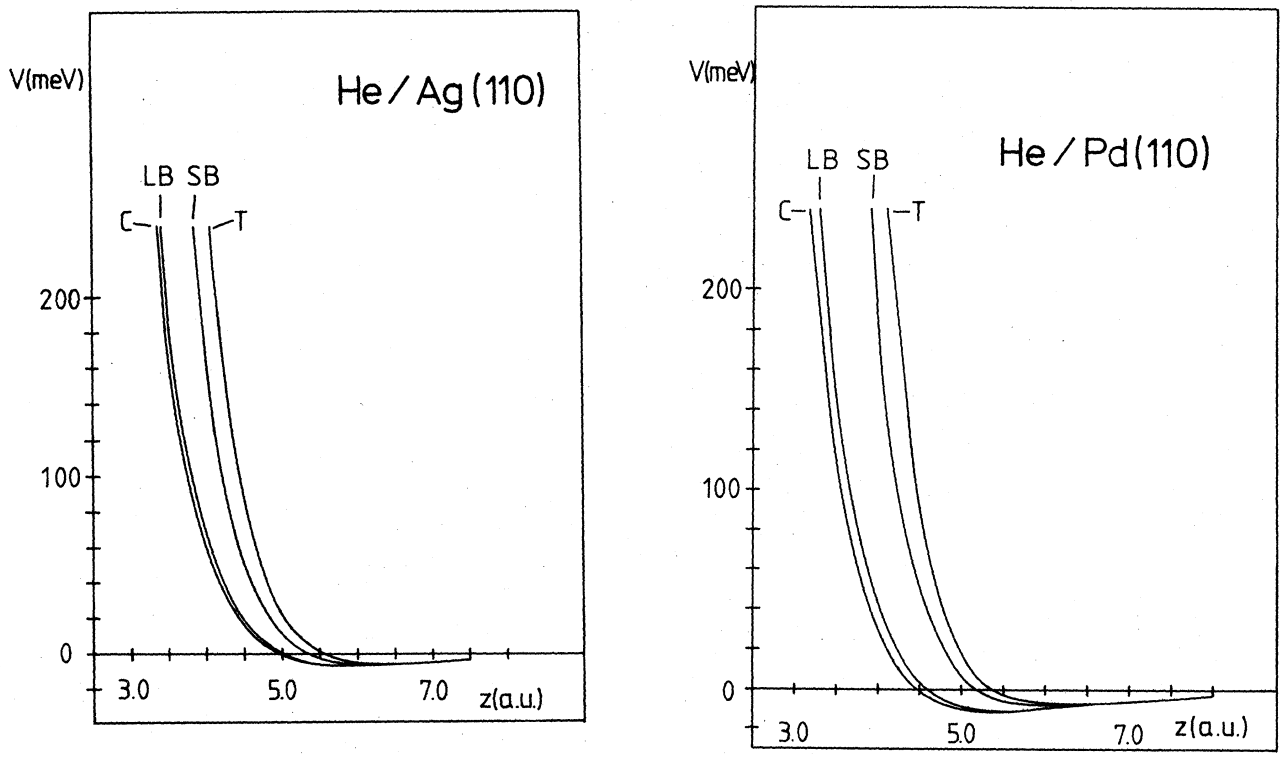

FIG. 5. (*Continued*).

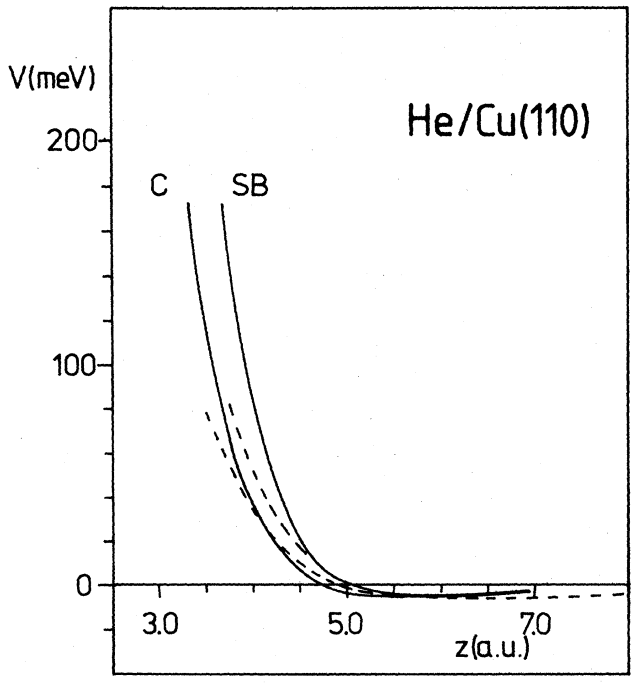

FIG. 6. Comparison between the model Hamiltonian potential-energy curves for He adsorption in the center and short-bridge positions of Cu(110) with the "experimental" potential-energy curves of Harris and Liebsch (Ref. 11).

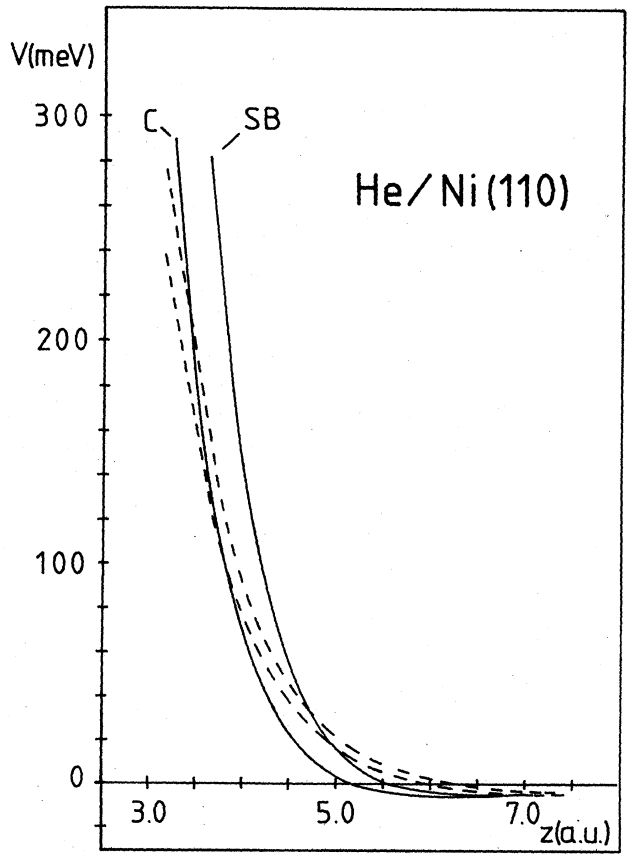

FIG. 7. Comparison of the potential fitted by Garcia, Barker, and Rieder (Ref. 37) (dashed curve) to the He/Ni(110) scattering data with the theoretical results (solid curve).

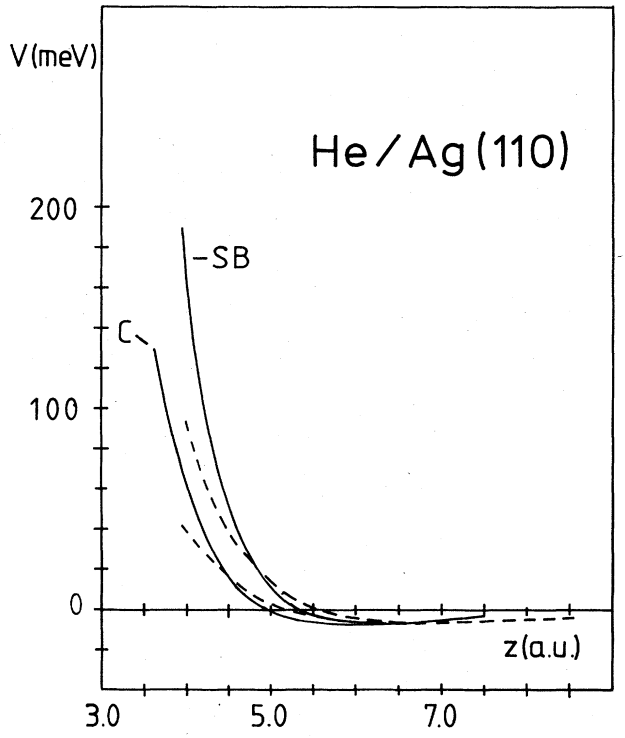

FIG. 8. Comparison of the theoretical and "experimental" potential-energy curves for He adsorption in the center and short-bridge positions on Ag(110). The "experimental" curves were derived by Schinke and Luntz (Ref. 7).

B. The theoretically predicted trends in comparison to the experimental evidence

The results of our calculations are summarized in Tables V—IX and compared to the available experimental data.

As far as qualitative trends are concerned the comparison is quite favorable. The major trends are as follows.

(i) Increase of well depth in the order He/Ni, He/Cu, He/Ag, and He/Pd and in the order Ne/Cu, Ne/Ni, Ne/Ag, and Ne/Pd, confirmed by experiment for He/Ag and He/Pd. The experimental value for He on copper is for the more open (115) and (113) faces where the helium atoms might possibly penetrate deeper into the surface feeling stronger attraction.

(ii) For helium, the corrugation increases in the order He/Ni, He/Cu (which is close to that of He/Ni), He/Ag, and He/Pd. For neon, however, Ni has a distinctively larger corrugation than Cu (increasing in the order Ne/Cu, Ne/Ni, Ne/Ag, and Ne/Pd). For helium the experimentally observed corrugations are found to increase in the order He/Cu, He/Ni (which is close to that of He/Cu), [He/Pd], and He/Ag. With the exception of Pd the trends are reproduced by the theory. However, Pd is the only case where only a fit to a hard corrugated wall (HCW) is available. If the scattering data would be fitted to a soft potential, it is very much to be expected that the corrugation will be found larger than for Ag. This expectation rests on the experience with the system He/Cu(110) (see below). For neon the corrugation on silver is not known. For the other metals the corrugation deduced from scattering data increases from Ni via Cu up to Pd

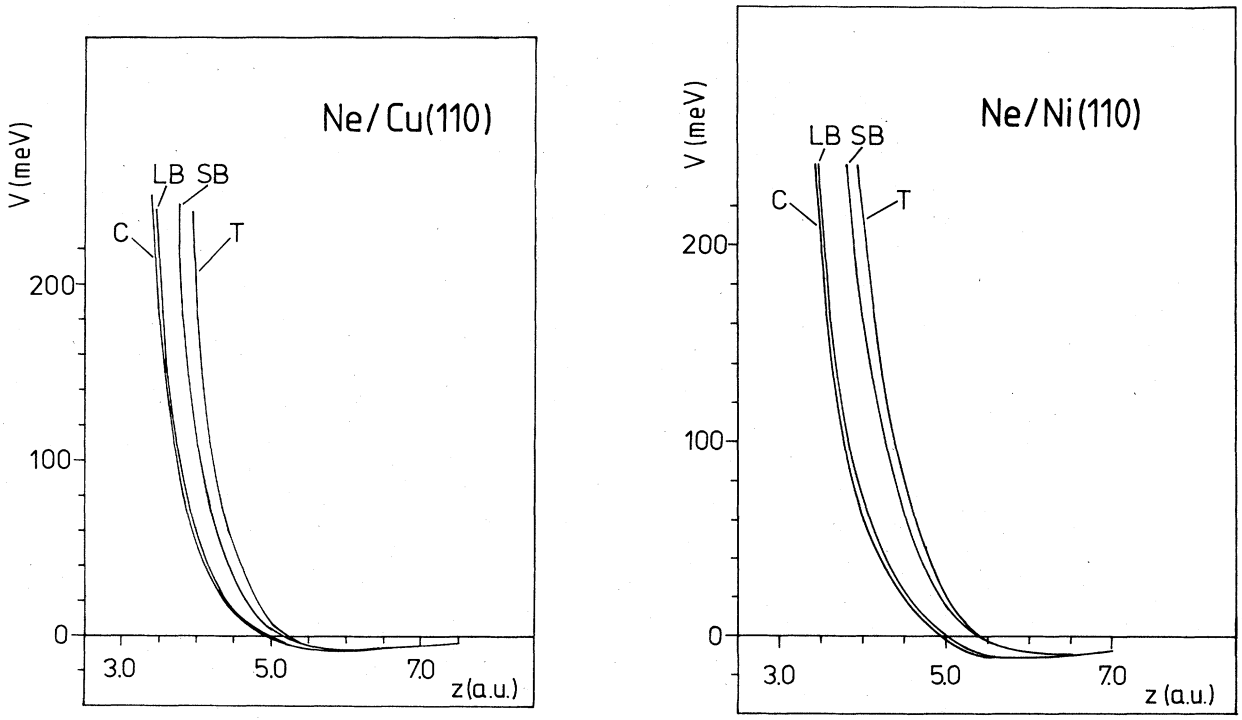

FIG. 9. Calculated potential-energy curves perpendicular to the (110) faces for adsorption of Ne above the four high-symmetry positions indicated in Fig. 4.

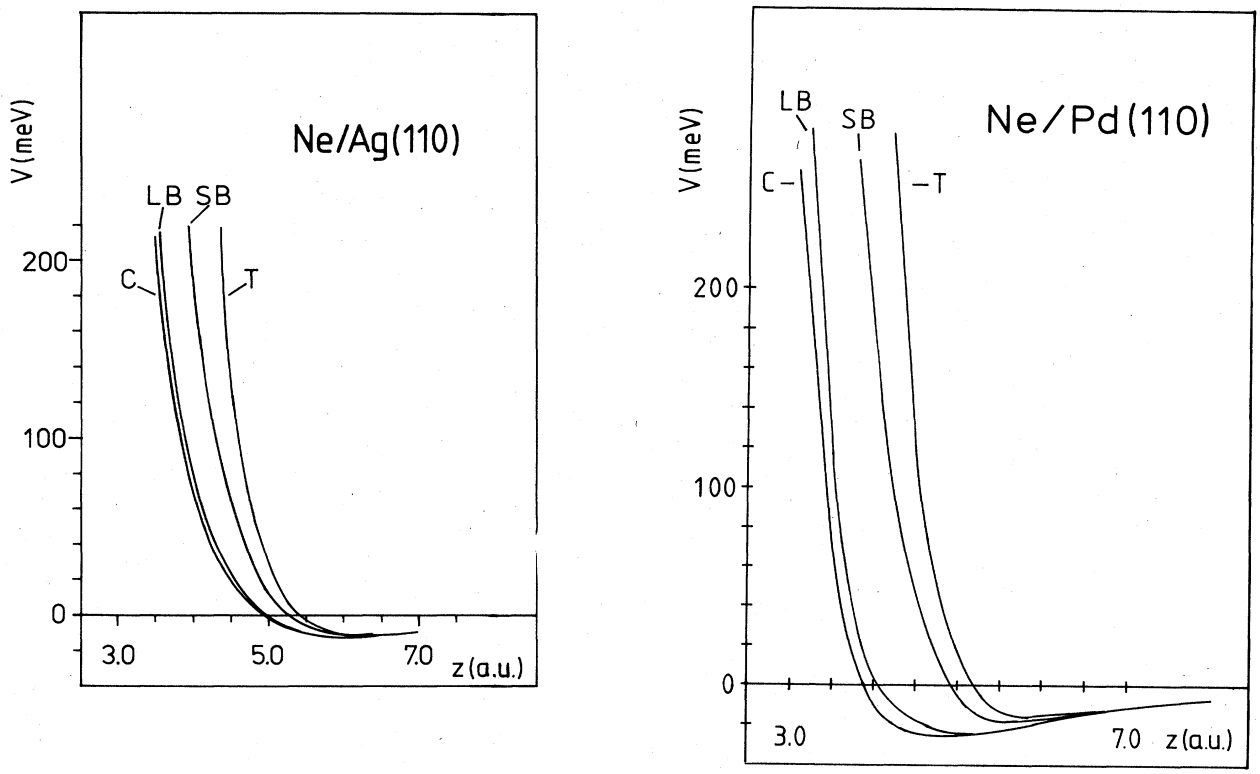

FIG. 9. (*Continued*).

(i.e., the qualitative trends for copper and nickel are apparently interchanged compared to the theory). Here, however, only the copper value has been deduced by a fit to a soft potential, the values for Ni and Pd apply to HCW fits.

(iii) The theoretically predicted increase of well depth from He to Ne is confirmed experimentally for the copper surfaces.

(iv) Increase of corrugation from He to Ne. This is confirmed by experiment for Cu(110), Ni(110), and Pd(110). The corrugations predicted by our theory do not appear to be quantitative. One has, however, to bear in mind that the quoted "experimental" values for Ne/Ni(110), Ne/Pd(110), and He/Pd(110) were derived by fitting the diffraction data to a HCW model. That this is a serious approximation can be appreciated, if in the case of He/Cu(110) one compares the HCW corrugation value of 0.09 bohr to the value derived from the Harris-Liebsch potential at $E_{\text{kin}\perp}=60$ meV, which is 0.23 bohr. The theoretically predicted corrugations are usually larger than those derived from experiment. One exception is He/Ag(110), where agreement is nearly perfect for small kinetic energies ($\lesssim 60$ meV), but theory predicts too small values for higher kinetic energies. The other exception is Ne/Cu(110). Possible explanations for these deviations are offered in Sec. VI.

(v) The softness parameters for He, defined as the logarithmic derivatives of the potential, increase from Ag via Ni and Cu to Pd for energies of incidence less than 120 meV. This is the tendency displayed by the experimentally determined softness parameters, namely increasing in the order He/Ag, He/Ni, and He/Cu,[4,5,38] though the model Hamiltonian potentials are generally less soft than the experimental ones.

C. Corrugation functions and their energy dependence

Another point of concern are the deviating experimental results for He/Ni(110). This problem was already met in the work by Garcia, Barker, and Batra,[12] who found that a fit to experiment requires a corrugation in the less-closed-packed [100] direction, which is unusually small (about 0.14 bohr) and independent of energy between 14 and 80 meV.

In this connection it it interesting that our calculations indeed predict the corrugation for He/Ni(100) to be nearly independent of energy between 20 and 200 meV although the magnitude is more than 2 times larger than the experimental value (cf. Fig. 10). For He/Cu(110) our theory yields an energy-dependent corrugation, which increases slightly between 20 and 200 meV (cf. Fig. 10).

The corrugations for He/Pd(110) and He/Ag(110) show in our theory a slight increase from 20 to 200 meV (Fig. 11). For neon scattering our calculations predict qualitatively similar trends for the energy dependence of the corrugation. Ne on Pd(110) and Ni(110) makes an exception from this behavior. The corrugation amplitude in the less-close-packed $z(01)$ direction is predicted to decrease at higher energies of incidence (cf. Fig. 11).

The calculation of whole potential-energy surfaces

TABLE V. Equilibrium distances (R_{eq}, a.u.) and potential well depths (D, meV) for helium and neon adsorption above the four high-symmetry points from Fig. 1 on Cu, Ag, Ni, and Pd(110) surfaces. Experimental data for the potential well depths are referred to for comparison with the numerical results.

Geometric position \ Metal	Cu	Ag	Ni	Pd
		R_{eq} (a.u.)		
	Helium			
On top	6.0	6.5	6.5	6.0
Short bridge	6.0	6.3	6.5	6.0
Long bridge	5.5	6.0	6.0	5.5
Center	5.5	6.0	6.0	5.5
	Neon			
On top	6.0	6.5	6.5	6.0
Short bridge	6.0	6.5	6.5	5.5
Long bridge	6.0	6.0	6.0	5.0
Center	6.0	6.0	6.0	5.0
		D (meV)		
Geometric position \ Metal	Cu	Ag	Ni	Pd
	Helium			
On top	5.0	5.4	4.3	7.5
Short bridge	5.2	5.6	4.4	8.2
Long bridge	5.7	6.5	5.2	11.0
Center	5.8	6.6	5.2	11.4
Expt.	6.35[a]	6.0		8.05
Reference	4	38		8
	Neon			
On top	6.9	10.3	8.3	15.8
Short bridge	7.1	10.5	8.4	17.7
Long bridge	7.4	11.4	10.3	23.9
Center	7.4	11.5	10.4	25.7
Expt.	12.1			
Reference	23			

[a]Heat of helium adsorption on Cu(113) and Cu(115).

represents no special difficulty for the model-Hamiltonian approach, the high symmetry of the studied system being no restriction at all. Cross sections of such potential-energy surfaces at different energies along the [10] and [01] directions of the (110) face of Pd are displayed in Figs. 12 and 13 for He and Ne, respectively. These equipotential curves allow to trace the energy dependence of the corrugation amplitudes. They are separately plotted in Fig. 10 and 11 as a function of energy.

The major trends are as follows.

(1) A slight increase of corrugation amplitudes of He on Pd(110) with energy for paths through the center of the unit cell.

(2) A slight increase of $z(10)$ and a decrease of $z(01)$ for Ne/Pd(110). Such a decrease is also observed for Ne on Ni(110) and could be ascribed to the strong increase in repulsion due to the extended d wave functions. As far as the corrugation functions are concerned the usual practice is to write them as Fourier series over the reciprocal-lattice vectors and then to keep only the first terms in the expansion. This approximation was tested by plotting the functions

$$\zeta(x,0)=\tfrac{1}{2}z(10)\cos\left[\frac{2\pi}{a}x\right],$$

$$\zeta(0,y)=\tfrac{1}{2}z(01)\cos\left[\frac{2\pi}{b}y\right]$$

as dashed lines in Figs. 12 and 13. Obviously, keeping only the first terms in the Fourier expansion of the corrugation function is a reasonable approximation for the less-corrugated crystal direction [10]. However, for the strongly corrugated [01] direction higher Fourier components are important.

TABLE VI. Classical turning points (R_{CT}, a.u.) and corrugation amplitudes z (a.u.) for helium and neon above Cu(110) in the close-packed [10] and less close-packed [01] directions compared with experimental data, where available, for perpendicular kinetic energies 60 and 240 meV.

	60 meV					240 meV				
Geometric position	R_{CT} (a.u.)	$z(10)$ (a.u.) Theory	Expt., Ref.	$z(01)$ (a.u.) Theory	Expt., Ref.	R_{CT} (a.u.)	$z(10)$ (a.u.) Theory	Expt., Ref.	$z(01)$ (a.u.) Theory	Expt., Ref.
					He/Cu(110)					
On top	4.25					3.68				
Short bridge	4.12	0.13[a]		0.32	0.26	3.49	0.19		0.35	
			≈0.0		4					0.38
Long bridge	3.82	0.02	31	0.43		3.21	0.07		0.47	4
Center	3.80					3.14				
					Ne/Cu(110)					
On top	4.45					3.92				
Short bridge	4.27	0.18		0.32	0.43	3.75	0.17		0.34	
Long bridge	3.98	0.03		0.47	23	3.44	0.03		0.48	
Center	3.95					3.41				

[a]The two theoretical values are for trajectories of the noble-gas atom above the rows of metal atoms (larger corrugation amplitude) and in between the rows (smaller z values).

TABLE VII. Classical turning points (R_{CT}, a.u.) and corrugation amplitudes z (a.u.) for helium and neon above Ag(110) in the close-packed [10] and less-close-packed [01] directions compared with experimental data, where available, for perpendicular kinetic energies 60 and 180 meV.

	60 meV					180 meV				
Geometric position	R_{CT} (a.u.)	$z(10)$ (a.u.) Theory	Expt., Ref.	$z(01)$ (a.u.) Theory	Expt., Ref.	R_{CT} (a.u.)	$z(10)$ (a.u.) Theory	Expt., Ref.	$z(01)$ (a.u.) Theory	Expt., Ref.
					He/Ag(110)					
On top	4.65					4.18				
Short bridge	4.43	0.22	$\simeq$0.0	0.44	0.51	3.95	0.23		0.49	0.85
Long bridge	4.05	0.06	7, 38	0.60	38	3.52	0.06		0.66	7
Center	3.99					3.46				
					Ne/Ag(110)					
On top	4.79					4.41				
Short bridge	4.53	0.26		0.46		4.02	0.39		0.46	
Long bridge	4.12	0.05		0.67		3.62	0.06		0.79	
Center	4.07					3.56				

TABLE VIII. Classical turning points (R_{CT}, a.u.) and corrugation amplitudes z (a.u.) for helium and neon above Ni(110) in the close-packed [10] and less-close-packed [01] directions compared with experimental data, where available, for perpendicular kinetic energies 60 and 180 meV.

	60 meV					180 meV				
Geometric position	R_{CT} (a.u.)	$z(10)$ (a.u.) Theory	Expt., Ref.	$z(01)$ (a.u.) Theory	Expt., Ref.	R_{CT} (a.u.)	$z(10)$ (a.u.) Theory	Expt., Ref.	$z(01)$ (a.u.) Theory	Expt., Ref.
					He/Ni(110)					
On top	4.52					3.96				
Short bridge	4.44	0.08	0.06	0.37	0.14	3.88	0.08	0.08	0.39	0.12
Long bridge	4.13	0.05	5	0.39	5	3.54	0.05	12	0.42	12
Center	4.07					3.49				
					Ne/Ni(110)					
On top	4.63					4.08				
Short bridge	4.53	0.10	0.06—0.08	0.51	0.29	3.94	0.14		0.41	
Long bridge	4.08	0.06	8	0.55	8	3.57	0.04		0.51	
Center	4.02					3.53				

TABLE IX. Classical turning points (R_{CT}, a.u.) and corrugation amplitudes z (a.u.) for helium and neon above Pd(110) in the close-packed [10] and less-close-packed [01] directions compared with experimental data, where available, for perpendicular kinetic energies 60 and 180 meV.

	60 meV					180 meV				
Geometric position	R_{CT} (a.u.)	$z(10)$ (a.u.) Theory	Expt., Ref.	$z(01)$ (a.u.) Theory	Expt., Ref.	R_{CT} (a.u.)	$z(10)$ (a.u.) Theory	Expt., Ref.	$z(01)$ (a.u.) Theory	Expt., Ref.
					He/Pd(110)					
On top	4.65					4.27				
Short bridge	4.45	0.20	0.04	0.68	0.40	4.01	0.26		0.69	
Long bridge	3.88	0.11	8	0.77	8	3.43	0.11		0.84	
Center	3.77					3.32				
					Ne/Pd(110)					
On top	4.72					4.41				
Short bridge	4.44	0.28	0.08	0.90	0.60	4.02	0.39		0.75	
Long bridge	3.67	0.13	8[a]	1.05	8[a]	3.42	0.15		0.99	
Center	3.54					3.27				

[a]For $E_{kin\perp}=63$ meV (HCW).

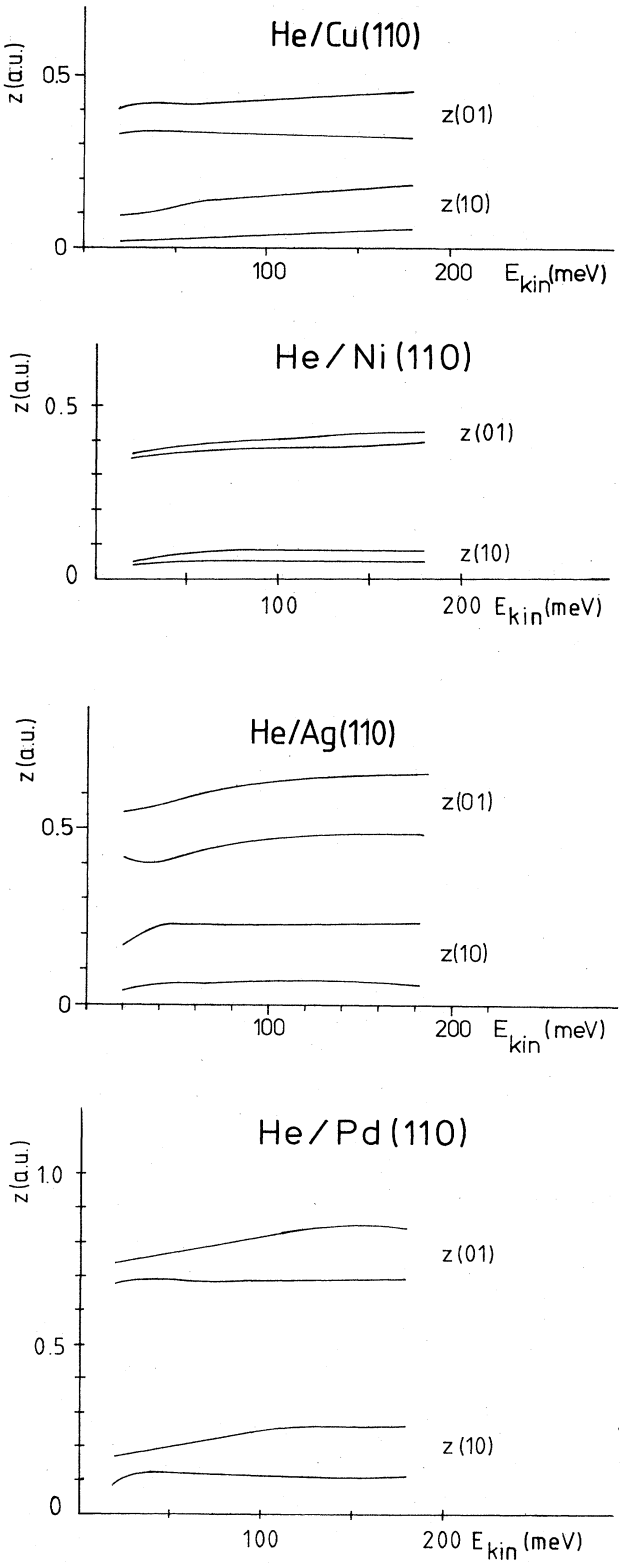

FIG. 10. Energy dependence of the corrugation amplitudes for helium. $z(01)$ and $z(10)$ are the corrugations in the less-close-packed and the close-packed direction, respectively. The upper curve of each pair corresponds to a path through the center of the unit cell, the lower curve applies for paths passing on top of metal atoms in the first layer.

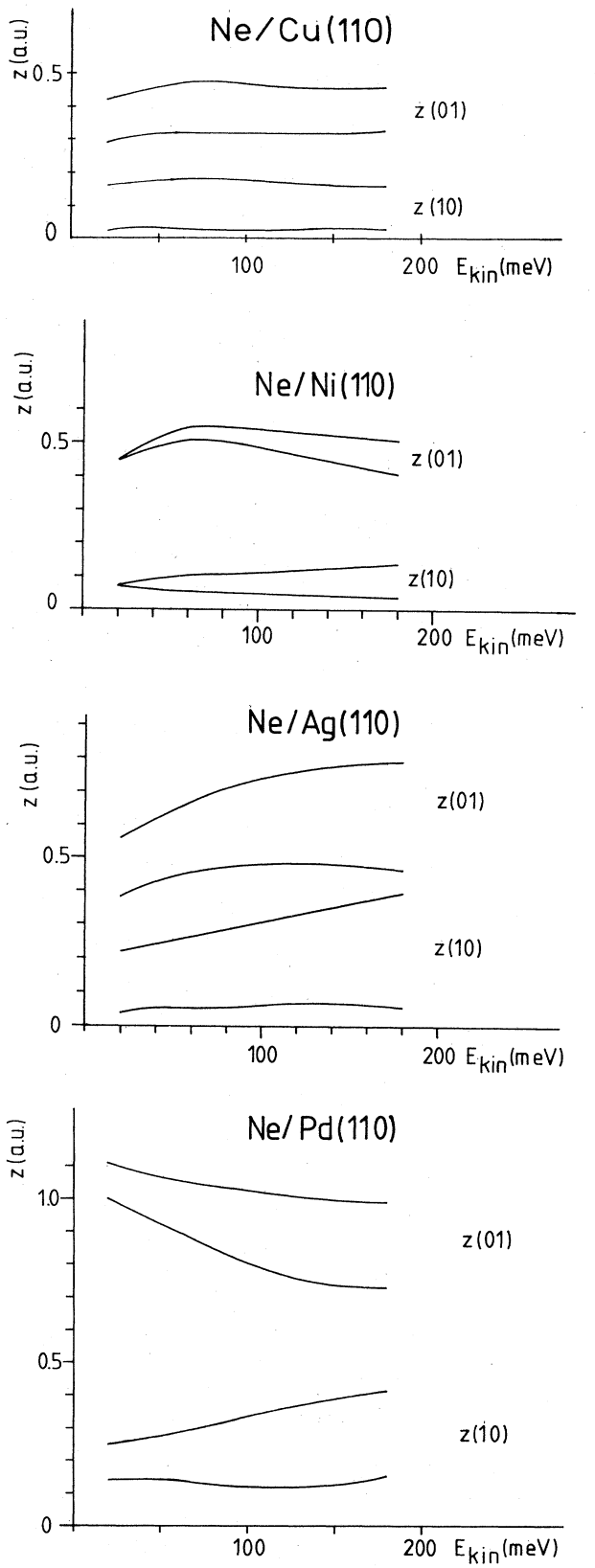

FIG. 11. Energy dependence of the corrugation amplitudes for neon. See legend to Fig. 10 for explanation of different curves.

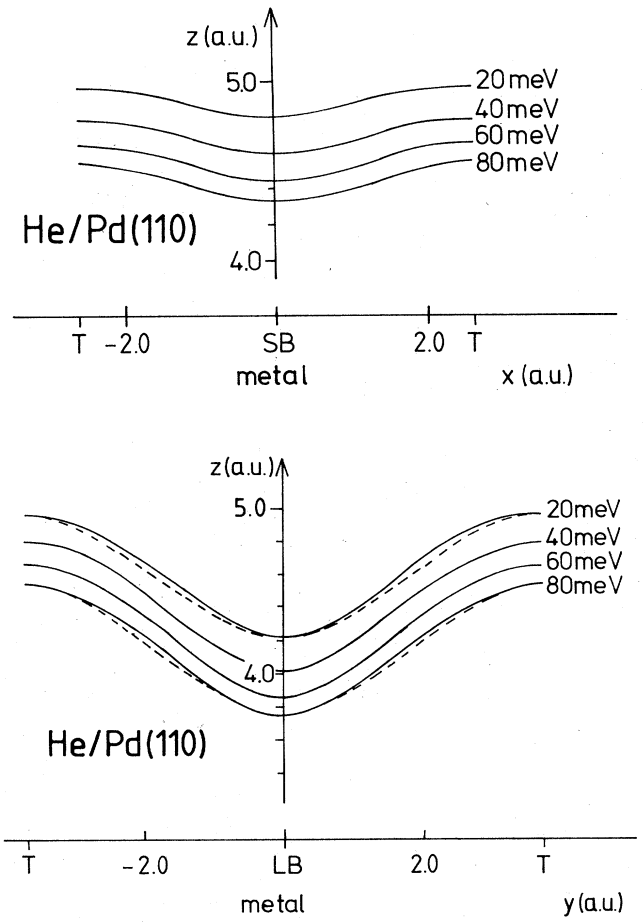

FIG. 12. Equipotential curves for He/Pd(110) concerning the movement of the He atom along the close-packed [100] (short bridge to on top), and less-close-packed [010] direction (long bridge to on top), respectively. The first Fourier components of the corrugation functions $\zeta(x,0)$ and $\zeta(0,y)$ are plotted as dashed curves.

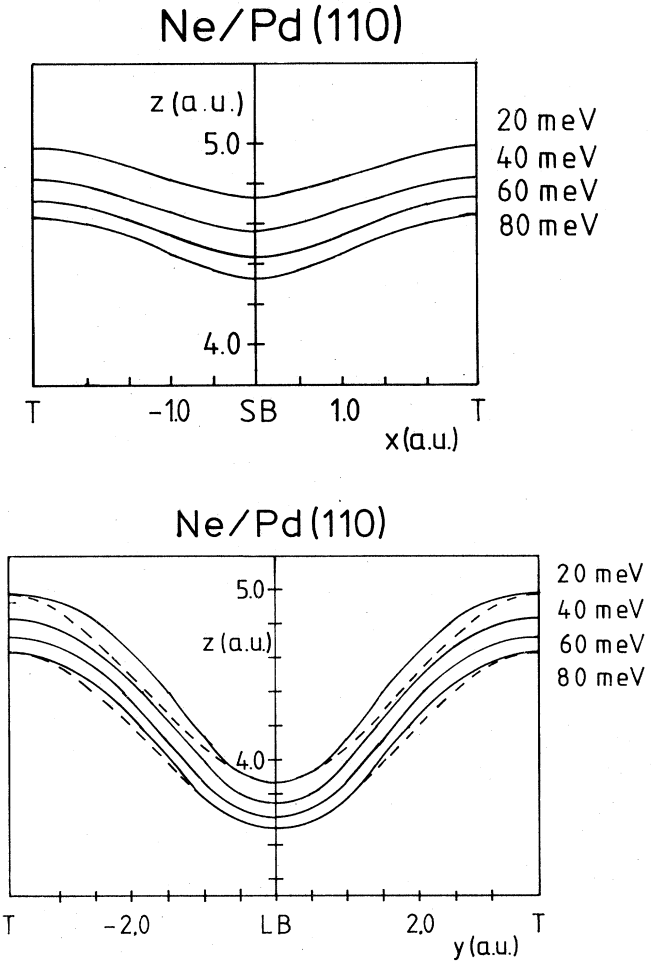

FIG. 13. Equipotential curves as described in the legend to Fig. 12 for Ne/Pd(110).

VI. DISCUSSION

The discussion serves several purposes. It enables us to (1) explain theoretically predicted trends physically, (2) point out possible deficiencies of our theory and connect these tentatively to discrepancies with experimental data, (3) check our predictions against reasonable variations of the properties and parameters assumed for the asymptotically *separated* gas-atom—metal system, and (4) derive an approximate analytic formula for the He-metal potential, which elucidates the physics. We start with the last point in order to reveal the physical picture behind the model Hamiltonian and the numerical calculations.

A. An approximate analytical formula for the He—transition-metal potential

1. Contributions due to the electronic interaction with the occupied metal states

The discussion is facilitated if a discretization into only two adsorbate-projected metal states—one occupied, the other empty—is considered. First consider only the coupling of gas-atom orbitals to the occupied metal state. According to Ref. 25 this gives no net change of the electronic energy. That it is not repulsive is a consequence of the exchange hole formed in the metal. Up to second order in the overlap the exchange energy for helium is $-3/2S_0^2U(z)$, where S_0 is the overlap of the $1s$ orbital with the occupied metal state and $U(z)$ is the image-force-renormalized Coulomb integral. Near the classical turning point for He/Pd ($z=4$ a.u.) the exchange energy is -253 meV, near the minimum it is ~ -3 meV.

Another attractive contribution is the GMS potential felt by the metal electrons. It is of the order $-2S_0^2U(z)$ for helium. The helium $1s$ orbital contracts due to mixing with the occupied metal states. This increases the electron-electron repulsion on the helium by

$$\Delta E_{A-A}^{\text{rep}} = \tfrac{1}{2}S_0^2U(z) .$$

The gross repulsion between adelectrons and metal electrons neglecting exchange is $3S_0^2U(z)$. If we add the four previously-discussed contributions, we get

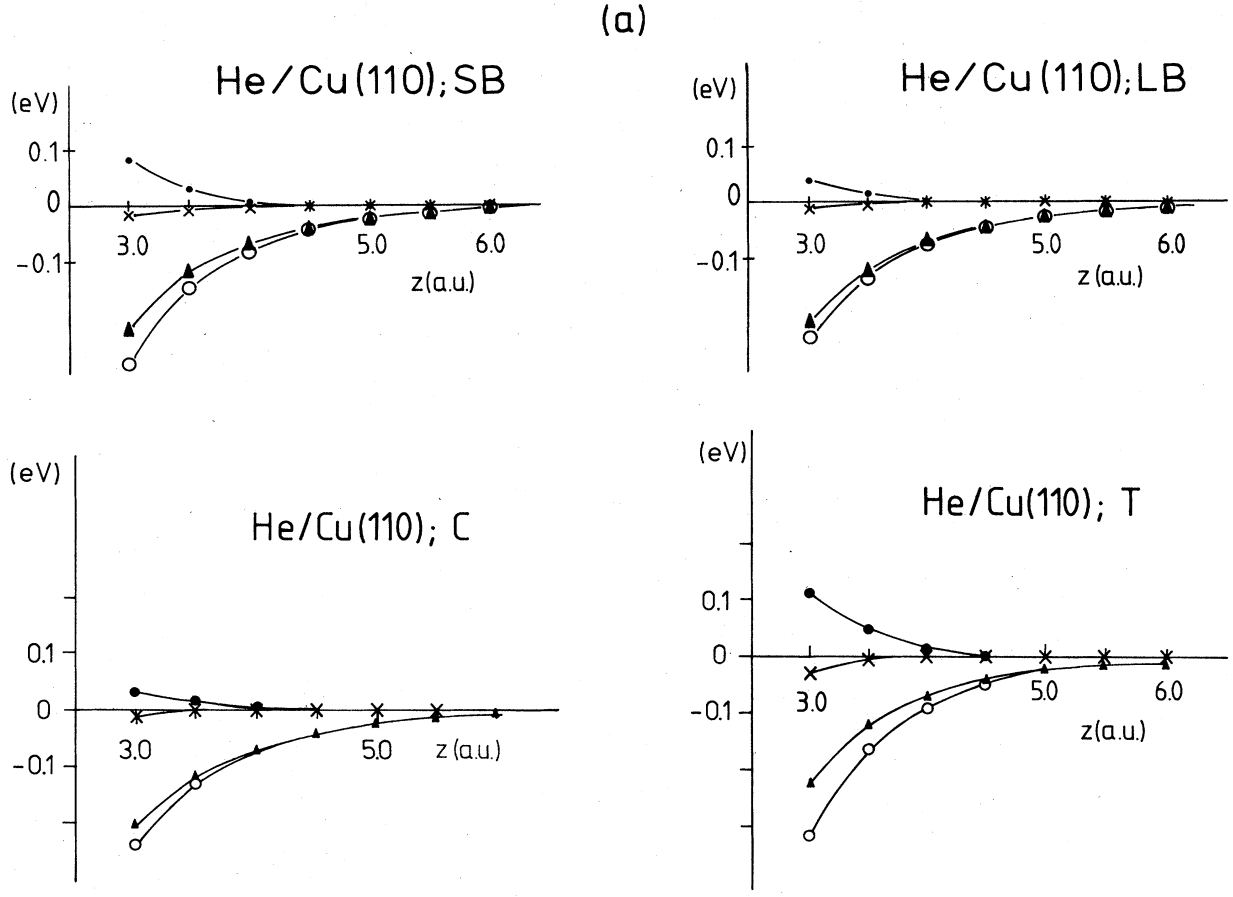

FIG. 14. (a) Contributions to the electronic interaction energy for He/Cu(110). Compare text for explanation of plotted quantities: ●, E_M^{IF} [cf. Eq. (36)]; ×, ΔG_{occ}; ▲, $\Delta G_{\mathrm{el}}(z)+\Delta G_{\mathrm{occ}}=E_M^{\mathrm{IF}}+E_{1s}^{\mathrm{IF}}+\Delta G_{\mathrm{occ}}$; ○, E_{1s}^{IF} [cf. Eq. (33)]. (b) Repulsive part of the He/Cu(110) potential and its components: ●, $E_{\mathrm{GMS}}^{\mathrm{rep}}=2S_0^2U(z)$ [cf. Eq. (37)]; ×, V_{dipole}; ▲, $E^{\mathrm{rep}}=E_{\mathrm{GMS}}^{\mathrm{rep}}+V_{\mathrm{dipole}}$ [cf. Eq. (6)].

$$\Delta G_{\mathrm{occ}}=\Delta E_{A-A}^{\mathrm{rep}}+E_x+E_{A-M}^{\mathrm{rep}}+E_{\mathrm{GMS}}^{\mathrm{attr}}$$
$$=(\tfrac{1}{2}-\tfrac{3}{2}-2+3)S_0^2U(z)=0\ . \quad (22)$$

The cancellation of these terms is not fortuitous. It depends, of course, on the parametrization of the model Hamiltonian and takes its justification from the success of the model to describe qualitatively correctly the gas-metal interaction. The cancellation occurs only up to second order in the overlap S_0^2. Higher orders lead to a net change of energy. The true quantity ΔG_{occ} including *all* orders of the overlap is plotted in Fig. 14 for He/Cu. The deviation of this quantity from zero is a measure of the importance of higher- (than second-) order terms.

2. *Contributions due to the electronic interaction with the unoccupied metal states*

The rare-gas orbitals are then coupled with renormalized core energy

$$E_A^0(z)\rightarrow E_A^0(z)+(E_A^0-E_M)S_0^2/4+\tfrac{3}{4}S_0^2U(z)$$
$$=E_A^0[1+(1-E_M/E_A^0)S_0^2/4]+\tfrac{3}{4}S_0^2U(z)\ , \quad (23)$$

and renormalized Coulomb integral

$$U(z)\rightarrow U(z)(1+S_0^2/2) \quad (24)$$

to the unoccupied part of the metal states. The coupling is renormalized as well, e.g.,

$$\tilde{a}^{\dagger}_{A\uparrow}\tilde{a}_{u\uparrow}\rightarrow\hat{a}^{\dagger}_{A\uparrow}\hat{a}_{u\uparrow}(1+\tfrac{3}{8}S_0^2)\ . \quad (25)$$

All these renormalizations, however, affect the total energy at most in order $S_0^2S_u^2$ and therefore are negligible.

The net gain in electronic energy comes now from the mixing with empty metal states and is equal to the change of the sum of $1s$ orbital energies:

$$\Delta G_{\mathrm{el}}(z)=2[E_A^0+U(z)-E_u]S_u^2/4\ . \quad (26)$$

This quantity is displayed in Fig. 14 as well. It consists of two repulsive and one attractive contributions. $-E_uS_u^2/2$ stems from the polarization of the $1s$ orbital towards the metal; charge is removed from the center of the helium core and thereby core-attraction energy is lost. The polarization is connected with a contraction (often called promotion) of the remaining part of the $1s$ charge density

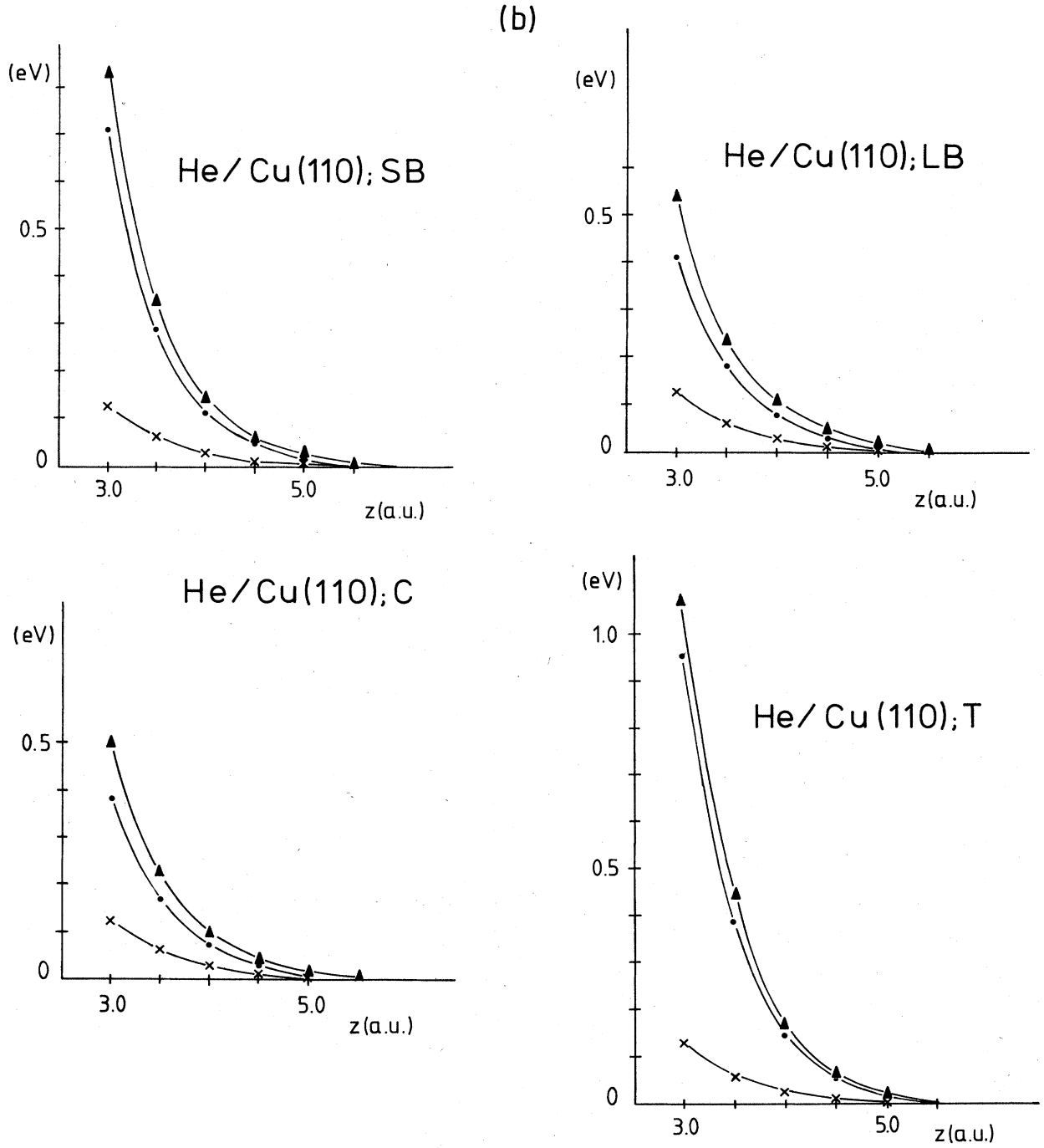

FIG. 14. (*Continued*).

around the helium core. This contraction implies an increase of the electron-electron repulsion by $U(z)S_u^2/2$. These repulsive contributions are, however, overcompensated by the gain in interference energy $E_A^0 S_u^2/2$ due to the formation of the "adsorption orbitals."

The terms $E_A^0 S_u^2$ and $-E_u S_u^2/2$ contain, of course, both the change in kinetic and in potential energy; the separation is, however, not exhibited in the notation of second quantization. The presented physical picture of the mechanism gaining electronic energy is very similar to Ruedenberg's interpretation of the chemical bond.[39]

3. *The core repulsion*

This contribution $E^{\text{rep}} = E^{\text{rep}}_{\text{GMS}} + V_{\text{dipole}}$ is given exactly by the term of H_2 of the Hamiltonian [Eq. (1)]. Together with its components it is plotted in Fig. 14 for He/Cu. It should be remembered that the terms $E^{\text{rep}}_{\text{GMS}}$ have been

constructed in such a way that *classically* ($\tilde{n}_{As}=1$; $\tilde{n}_{ks}=1$ for $|ks\rangle$ occupied), they would cancel exactly with the corresponding attractive terms, i.e., with the GMS attraction (the first term of H_1 of the Hamiltonian) and the electrostatic attraction of the adelectrons by the dipole potential. The latter is implicitly taken into account by making use of Eq. (6).

In the remainder of this paper the core repulsion will be made responsible for giving rise to the repulsive branch of the potential-energy curve. This interpretation is based on the cancellations leading to $\Delta G_{\rm occ}=0$ [cf. Eq. (22)].

Obviously this is not the only possible interpretation. For example, one could instead balance the core repulsion against the corresponding electrostatic attractive terms ($E^{\rm attr}_{\rm GMS}$ and $E^{\rm attr}_{A-\rm dipole}$) and then discuss the repulsive part of the total energy as arising from $\Delta E^{\rm rep}_{A-A}+E^{\rm rep}_{A-M}+E_x$. This would lead to the interpretation that in order to obey Pauli's exclusion principle the electron wave functions have to rearrange in such a way that the electron-electron repulsion becomes larger (exchange repulsion). This interpretation is physically as correct as the one we are pursuing in the following.

4. *Summary of energy contributions*

The weak rare-gas—metal—interaction energy can be discussed in terms of the squared overlaps S_0^2 and S_u^2:

$$S_0^2=\sum_k^{\rm occupied}|\langle 1s\,|\,k\rangle|^2=\sum_k^{\rm occupied}\left|\int d^3r\langle 1s\,|\,\mathbf{r}\rangle\langle\mathbf{r}\,|\,k\rangle\right|^2$$
$$=\sum_k^{\rm occupied}\left|\int\int d^3r'\int d^3r\langle 1s\,|\,\mathbf{r}\rangle\langle\mathbf{r}'\,|\,1s\rangle\langle k\,|\,\mathbf{r}'\rangle\langle\mathbf{r}\,|\,k\rangle\right|$$
$$=\int d^3r'\int d^3r\langle 1s\,|\,\mathbf{r}\rangle\langle\mathbf{r}'\,|\,1s\rangle\sum_k^{\rm occupied}|\langle k\,|\,\mathbf{r}'\rangle\langle\mathbf{r}\,|\,k\rangle|=\int d^3r'\int d^3r\langle 1s\,|\,\mathbf{r}\rangle\langle\mathbf{r}'\,|\,1s\rangle\rho(\mathbf{r}',\mathbf{r}),\tag{27}$$

where $2\rho(\mathbf{r}',\mathbf{r})$ is the Fock-Dirac density matrix of the unperturbed metal surface. For calculating S_0^2 summation is only over one spin orientation. With use of the mean-value theorem, S_0^2 can be approximated by

$$S_0^2=\langle\langle 1s\,|\,\mathbf{r}'\rangle\langle\mathbf{r}\,|\,1s\rangle\rangle_{\rm av}\int_{V_{1s}}d^3r'\int_{V_{1s}}d^3r\,\rho(\mathbf{r}',\mathbf{r})$$
$$=\langle\langle 1s\,|\,\mathbf{r}'\rangle\langle\mathbf{r}\,|\,1s\rangle\rangle_{\rm av}\bar{\rho}_0(\mathbf{r}_{\rm He})V_{1s}^2\,,\tag{28}$$

where $\bar{\rho}_0$ is the occupied metal charge density only, if the He $1s$ orbital can be considered extremely localized compared to the metal lattice constant, i.e., if $\langle\mathbf{r}\,|\,1s\rangle\approx\delta(\mathbf{r}-\mathbf{r}_{\rm He})$.

S_0^2 is then approximately proportional to the unperturbed metal electron charge density averaged over the volume occupied by the helium $1s$ charge density. Similarly one writes for S_u^2,

$$S_u^2=\langle\langle 1s\,|\,\mathbf{r}'\rangle\langle\mathbf{r}\,|\,1s\rangle\rangle_{\rm av}\bar{n}_0(\mathbf{r}_{\rm He})V_{1s}^2\,.\tag{29}$$

Here

$$\bar{n}_0(r)=\sum_k^{\rm unoccupied}|\langle k\,|\,\mathbf{r}\rangle|^2\tag{30}$$

is the local charge density of unoccupied states at the point $\mathbf{r}$. $\bar{n}_0$ approximates this quantity under the same conditions as mentioned above for $\bar{\rho}_0$. $\bar{n}_0$ is the energy integrated local density of states of the empty metal states between Fermi level and vacuum level. Note that the numerical calculations evaluate S_u and S_0 exactly and do not involve any "charge-density approximations." The discussion given here is for interpretational purposes only. If the proposed interpretations for $\bar{\rho}_0$ and $\bar{n}_0$ is valid, we recognize that each of the energy contributions we have been discussing is either proportional to the occupied or to the empty local metal density.

We then produce the following summarizations. Firstly, the attractive energy contributions: (i) exchange energy

$$E_x=-\tfrac{3}{2}S_0^2U(z)\propto\bar{\rho}_0(\mathbf{r}_{\rm He})\,,\tag{31}$$

(ii) GMS potential

$$E_{\rm GMS}=-2S_0^2U(z)\propto\bar{\rho}_0(\mathbf{r}_{\rm He})\,,\tag{32}$$

(iii) $1s$ interference energy,

$$E^{\rm IF}_{1s}=(S_u^2/2)[E_A^0(z)+U(z)-E_u(z)]$$
$$+(S_0^2/2)[E_A^0(z)+U(z)-E_0(z)]$$
$$=C_0\bar{\rho}_0(\mathbf{r}_{\rm He})+C_u\bar{n}_0(\mathbf{r}_{\rm He})\not\propto\bar{\rho}_0(\mathbf{r}_{\rm He})\,,\tag{33}$$

and (iv) image potential of He core, $-4/|z-z_{\rm im}|$. Secondly, the repulsive energy contributions: (i) Change of electron-electron repulsion on the helium atom,

$$\Delta E^{\rm rep}_{A-A}=\tfrac{1}{2}S_0^2U(z)\propto\bar{\rho}_0(\mathbf{r}_{\rm He})\,,\tag{34}$$

(ii) adelectron-metal electron repulsion,

$$E^{\rm rep}_{A-M}=3S_0^2U(z)\propto\bar{\rho}_0(\mathbf{r}_{\rm He})\,,\tag{35}$$

(iii) metal interference energy,

$$E^{\rm IF}_M=\tfrac{1}{2}S_0^2[E_0(z)-E_A^0(z)-U(z)]\propto\bar{\rho}_0(\mathbf{r}_{\rm He})\,,\tag{36}$$

(iv) GMS repulsion,

$$E^{\rm rep}_{\rm GMS}=2S_0^2U(z)\propto\bar{\rho}_0(\mathbf{r}_{\rm He})\,,\tag{37}$$

(v) core repulsion from the dipole layer,

$$E^{\rm rep}_{\rm dipole}=V_{\rm dipole}\propto\bar{\rho}_0(\mathbf{r}_{\rm He})\,,$$

and (vi) change of electronic energy due to image force, $4/|z-z_{\rm im}|$. Utilizing Eqs. (26) and (37), one obtains the

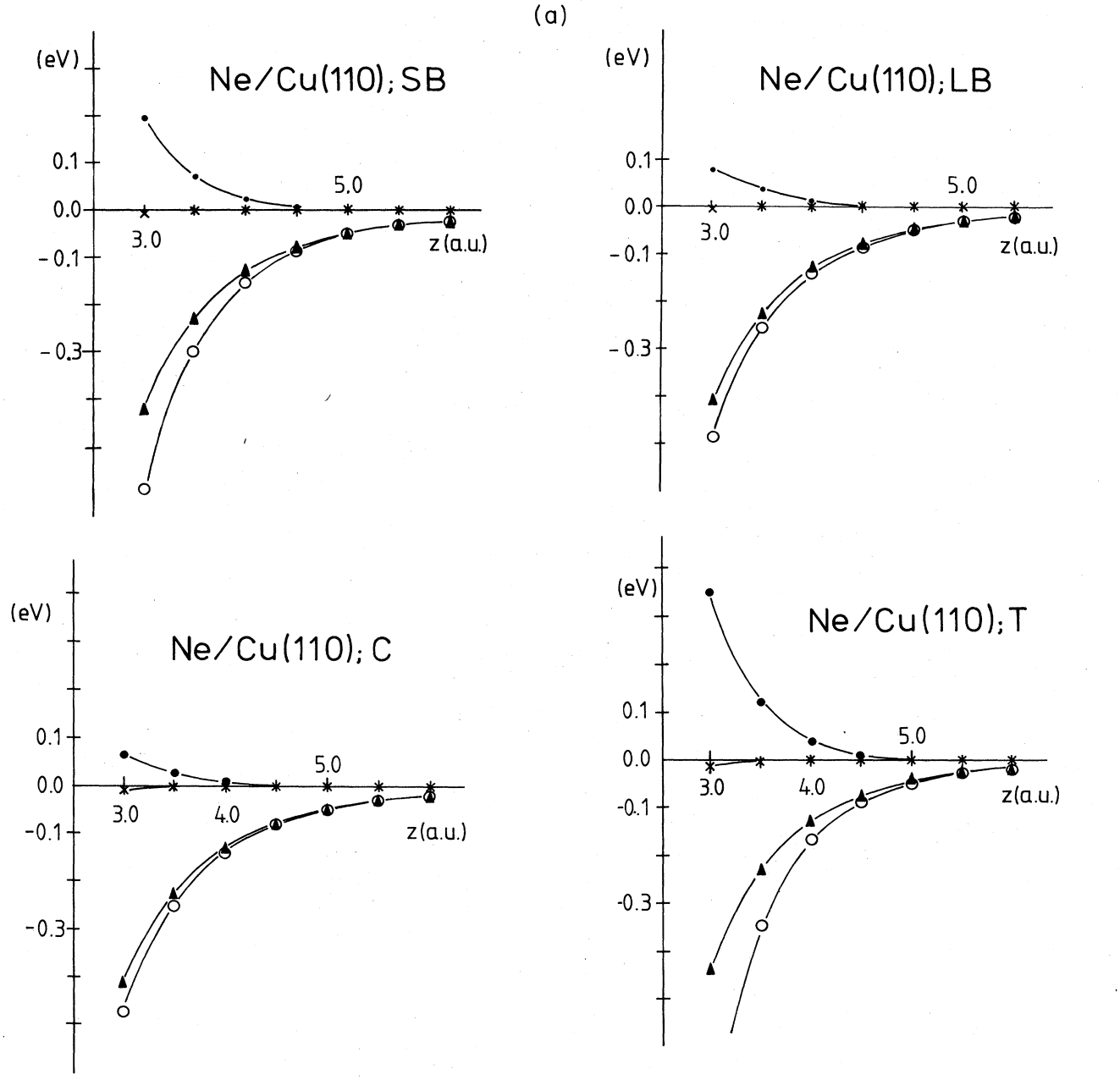

FIG. 15. Components of the total energy as described in the legend to Fig. 14 for Ne/Cu(110).

following simple expression for the potential-energy surface, which is correct to second order in the overlap:

$$V(\mathbf{r}_{\mathrm{He}})=\tfrac{1}{2}S_u^2[E_A^0(z)+U(z)-E_u]+2S_0^2U(z)+E_{\mathrm{dipole}}^{\mathrm{rep}} . \tag{38}$$

In Fig. 16 this approximate analytical expression is compared against the numerical result for the example of the He/Cu(110) on-top potential-energy curve. The excellent agreement demonstrates that the analytic formula may be used for interpretational purposes. The various contributions to the electronic energy are displayed in Figs. 14(a) and 15(a); the repulsive parts are plotted in Figs. 14(b) and 15(b).

From experiment only the total potential can be deduced. The same total potential can be decomposed into different attractive and repulsive parts. This has been demonstrated in the case of He/Cu(110),[19] where the Harris-Liebsch (HL) fit[11] and the Garcia, Barker, and Batra (GBB) fit[12] lead to essentially the same *total* potential, but both the repulsive and the attractive components considered alone are different. Up to ~40 meV the experimental potential agrees reasonably well with our theoretical one. It is now interesting to observe that in our theory

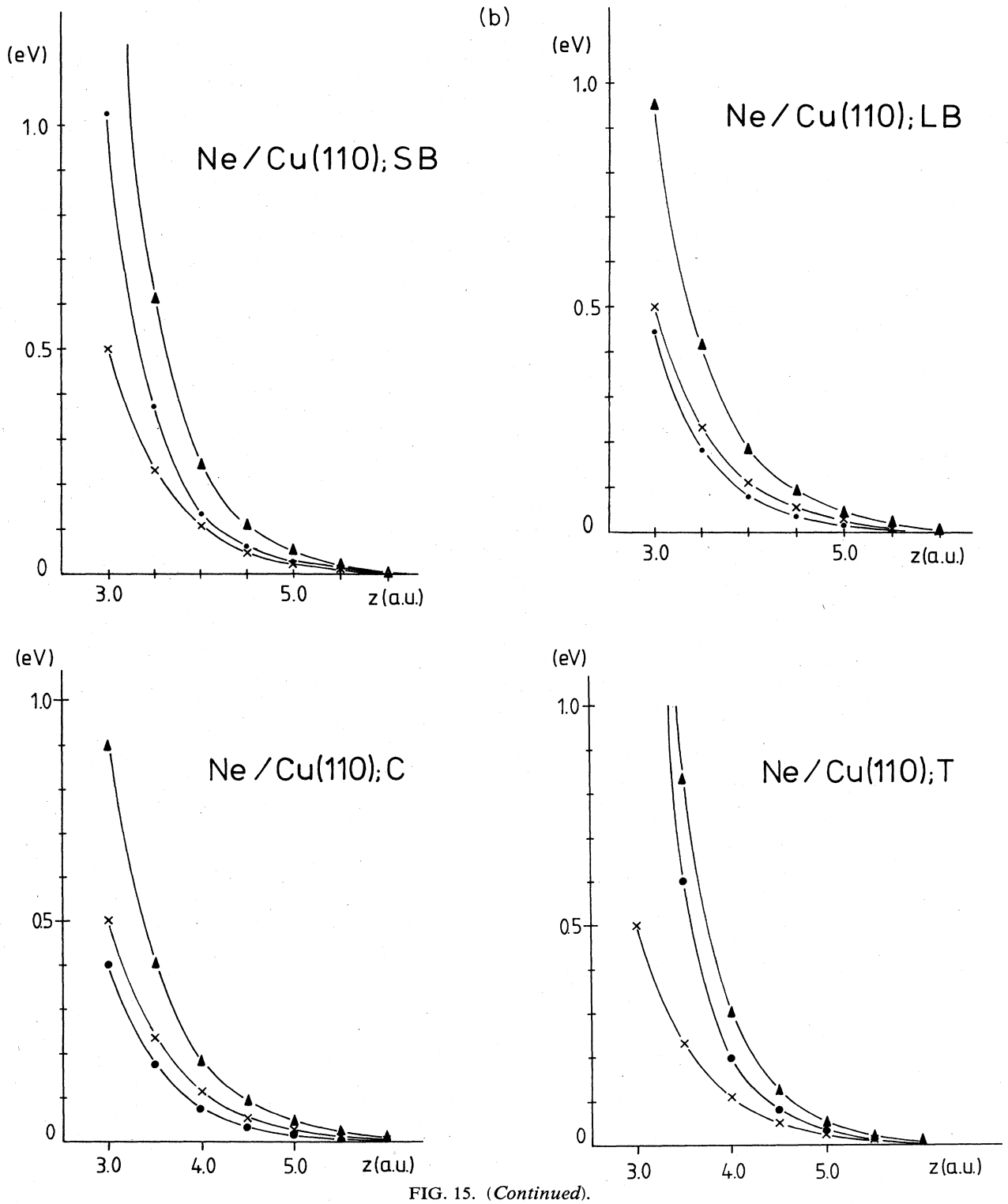

FIG. 15. (*Continued*).

both components (repulsive and attractive) vary significantly more rapidly than in both experimental fits.

At 40 meV, for example, we calculated

G_{el}(center) = −75 meV (HL, −68.6; GBB, −53.0),

G_{el}(SB) = −40 meV (HL, −54.0; GBB, −46.0),

V_{attr} = 30 meV (HL, 14.6; GBB, 7).

(The values for the experimental potentials are from Ref. 19 and correspond to E_z = 46 meV.) We have

corrugation of total potential, 0.35 a.u.

(*HL*, 0.25; *GBB*, 0.26),

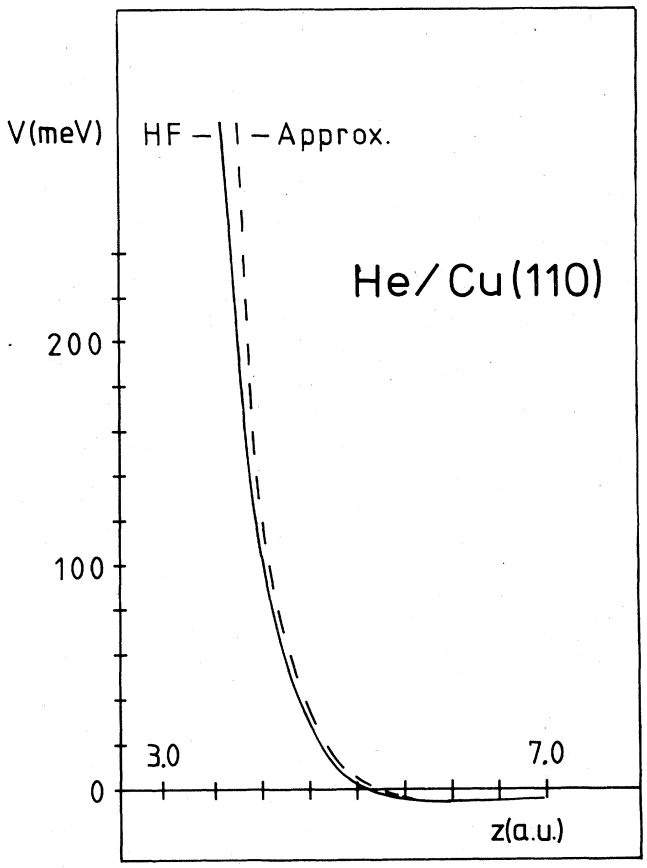

FIG. 16. Comparison between the results of a self-consistent calculation for helium on-top adsorption above Cu(110) diagonalizing the complete Hamiltonian (solid curve) and using the approximation Eq. (38) (dashed curve).

corrugation of repulsive potential, 0.27 a.u.

(*HL*, 0.1; *GBB*, 0.21) .

This means that for the Harris-Liebsch fit the repulsive part alone yields only 40% of the total corrugation, whereas for the GBB fit and in our theory it yields 80% of the total corrugation. In qualitative agreement with the discussion of Barker *et al.*[19] we also find that the corrugation is approximately proportional to the corrugation of the (occupied) metal charge density.

For neon the absolute magnitude and the variation of both components are calculated to be roughly twice as large as for helium. For the total corrugation the attractive part is of much higher importance than in the case of helium. For Ne/Cu(110) at 40 meV we find for the corrugation of the repulsive part alone 0.15 a.u., whereas the total corrugation is (center to short bridge) 0.30 a.u., i.e., the repulsive part along yields only 50% of the total corrugation. Note that the corrugation of the repulsive part alone is only half the value for helium. This appears plausible, if the Esbjerg-Nørskov density-potential proportionality is applied only to the repulsive part. The proportionality factors calculated by Puska, Nieminen, and Manninen[22] would then predict a much smaller corrugation for neon than for helium. The much larger interference energy for neon, however, changes the situation.

Compared to Salanon's experimental results,[23] our theory underestimates this effect. A possible explanation of this underestimation is the approximate and rather *ad hoc* treatment of the image force (see the discussion of "deficiencies" later on). The picture is the same for all metal surfaces. For neon the corrugation of the total potential is always roughly twice as large as that of the repulsive part only.

B. Physical explanation of the theoretically predicted trends

The discussion in the preceding section was restricted to the He-metal interaction. The physics is, however, completely analogous for neon. One only has to be careful with respect to the larger number of adsorbate orbitals involved. When this is important, it will be explicitly pointed out in the following.

All calculated trends can theoretically be explained by the competing interplay of the repulsion energy E^{rep} and the attractive interference energy $E^{\mathrm{IF}}=E_M^{\mathrm{IF}}+E_{1s}^{\mathrm{IF}}$. For He both contributions increase in absolute magnitude in the order He/Cu, He/Ni, He/Ag, and He/Pd. Generally the magnitudes of E^{IF} and E^{rep} are larger for Ne than for He. For neon the attraction $|E^{\mathrm{IF}}|$ increases in the order Ne/Cu, Ne/Ni, Ne/Ag, and Ne/Pd whereas the repulsive term $|E^{\mathrm{rep}}|$ increases (for center position) in the order Ne/Cu, Ne/Pd, Ne/Ni, and Ne/Ag. As demonstrated in the preceding section one can write approximately [cf. Eq. (38)]

$$V(\mathbf{r})\cong E^{\mathrm{rep}}(\mathbf{r})+E^{\mathrm{IF}}(\mathbf{r}) ,$$

$$E^{\mathrm{rep}}(\mathbf{r})\simeq\alpha\bar{\rho}_0(\mathbf{r}),\ E^{\mathrm{IF}}(\mathbf{r})\simeq\beta\bar{n}_0(\mathbf{r}) ,$$

where $\bar{\rho}_0$ is the *occupied* charge density at the metal surface and $\bar{n}_0$ is the empty charge density [cf. Eqs. (28), (29), and (30)]. α and β might be calculated from Eqs. (28) and (29). However, we did not calculate α and β explicitly, but it is obvious from Figs. 14 and 15 that they increase from He to Ne.

For the center position, neon penetrates deeper into the metal, because the attractive interference energy is larger for neon and the repulsive interaction with the d orbital sets in only at close distances. For the top position the repulsion is felt much earlier and the larger α^{Ne} value shifts the turning point for neon further out than for helium.

This explains the large corrugation of the neon potential for Ni and Pd. For copper and silver the interference energy has a smaller influence (because of the low copper and silver work functions) and the increased neon repulsion plays the dominant role. Therefore on copper and silver the neon turns round further out than helium for all geometries and the corrugations are approximately the same.

The reader should observe the important role played by the attractive interference energy. If it would be negligible, then neon would always penetrate less into the surface than helium (because $\alpha^{\mathrm{Ne}}>\alpha^{\mathrm{He}}$) and corrugation would be smaller for neon for all metal surfaces, as has been proposed before the experiments were performed.[22]

The gradient of the attractive interference energy in-

creases in the order Cu, Ni, Ag, and Pd. The same is true for the repulsive part, because the contraction of the d orbitals decreases in the indicated order so that the overlap S_0^2 becomes larger. Hence the predicted corrugation increases for helium from He/Ni and He/Cu via He/Ag to He/Pd and for Ne in the order Ne/Cu, Ne/Ni, Ne/Ag, and Ne/Pd.

C. Comparison of different metal surfaces

The quantities which vary significantly with the nature of the surface are the following.

(i) The GMS core repulsion; it increases from Cu via Ni and Ag to Pd. This is mainly due to the overlap with the d orbitals; the contraction increases in the order Pd, Ag, Ni, and Cu so that the repulsion is felt earlier for Pd than for Cu. There is also a small counterbalancing contribution from the hybridization gap, which is larger and at higher energies for Ni and Pd than for Cu and Ag; the hybridization gap decreases the core repulsion.

(ii) The interference energy E^{IF}, which increases from Cu via Ni and Ag to Pd. The increase runs parallel to the trend of the overlap with the unoccupied metal wave functions which is largest for Pd. A larger overlap S_u^2 means more empty metal wave functions to couple to or a better possibility for the noble-gas electrons to polarize towards the metal surface. Polarization comes about by virtual excitations into unoccupied states. This comes into effect only at closer distances to the surface, as a consequence of which the equilibrium distances are closer for Pd than for Ni, Ag, and Cu. The increased interference energy is responsible for the deeper potential minimum. The simultaneously increased core repulsion is not able to counterbalance this completely.

According to Eq. (38) the form of the potential-energy curve can roughly be understood as the superposition of two contributions: the attractive interference energy due to coupling to the *empty* metal density of states and the repulsive energy due to coupling to the occupied metal density of states.

The empty states reach out far from the surface. They have a small exponent for decay into the vacuum. The occupied states decay, however, much faster with a larger exponent. Therefore the attractive interference energy is felt at larger distances from the surface. It sets in first, but then increases only relatively slowly. The repulsive energy becomes important at closer distance, but then increases fast (due to the larger exponent of decay) and finally overcompensates the attractive interference energy, giving rise to the repulsive branch of the potential-energy curve.

D. Comparison of helium and neon

For neon, eight electrons ($2s^2 2p^6$) are included explicitly in the calculation. The $1s$ electrons are considered nonpolarizable so that the neon-ion core has an effective charge of $+8e$. It turns out that for a qualitative discussion only the $2s$ and $2p_z$ electrons have to be considered (the z direction is perpendicular to the surface). The contribution of the $2p_{x,y}$ electrons is negligible. The $2s$ orbital is the only one which has a significant overlap with the empty metal states, this overlap always being very similar to the overlap of the helium $1s$ orbital at the same distance. The unoccupied metal states have a rather slow exponential decay into the vacuum. The adorbitals only probe the exponential tail of the sp wave functions because of the large equilibrium distance from the surface. Due to the odd parity of the $2p_z$ orbital its overlap with the unoccupied part is considerably smaller than that of the $2s$ orbital.

Therefore, the attractive interference energy for neon arises nearly exclusively from the $2s$ empty-metal-states interaction. The observation, that despite the similar overlap the interference energy is much larger (roughly a factor of 2) for neon than for helium, is an interesting quantum-mechanical effect involving the nonorthogonality and the different effective electron potentials for neon and helium. It can be understood, if perturbation theory is applied to estimate the interference energies *after* the charge-density—bond-order matrix has been iterated to self-consistency.

The coefficient with which the empty metal state $|k\rangle$ is mixed into the adorbital $|A\rangle$ is in first order given by

$$C_{Ak}=\frac{V_{Ak}-E_A\langle A\,|\,k\rangle}{E_A-E_k}\,, \tag{39}$$

where E_A, E_k are here the self-consistently calculated one-electron energies. V_{Ak} is the effective self-consistent one-electron hopping matrix element:

$$V_{Ak}\cong\frac{E_A+E_k}{2}\langle A\,|\,k\rangle\,. \tag{40}$$

This yields for the coefficient

$$C_{Ak}\cong-\langle A\,|\,k\rangle/2\,, \tag{41}$$

which in first order is independent of the one-electron energies. The corresponding contribution to the interference energy is in first order given by

$$E_{Ak}^{\mathrm{IF}}\cong\frac{|\,V_{Ak}-E_A\langle A\,|\,k\rangle\,|^2}{E_A-E_k}=|\,\langle A\,|\,k\rangle\,|^2(E_A-E_k)/4\,, \tag{42}$$

which becomes more attractive for more tightly bound adorbitals (more negative E_A).

$$E_A(\mathrm{Ne}\ 2s)/E_A(\mathrm{He}\ 1s)\cong 2\,,$$

which explains the increased interference energy for neon. Despite the larger core attraction felt by the Ne $2s$, it is spacially as extended as the He $1s$, and therefore can mix as effectively as the He $1s$, gaining at the same time much more interference energy. The neon $2p_z$ overlaps significantly only with the d orbitals. This increases the GMS core repulsion considerably for neon. Also the core repulsion from the dipole potential is enhanced due to the larger core charge. These effects tend to compensate the larger interference energy at closer distances to the surface. The net outcome is, however, a deeper potential minimum for neon.

E. Possible deficiencies of the theory

If one wants to speculate on the reason for the too large He/Ni(110) corrugation as compared to experiment, one could mention several points.

(i) Our theory assumes the whole d-electron density of states (DOS) to be occupied. For Ni and Pd, $\sim 5\%$ of the DOS is empty. This error should lead to an overestimated corrugation. It would, however, apply to Pd as well, where agreement between theory and experiment appears to be better.

(ii) Existence of occupied surface states for Ni(110) of predominantly sp character, which reach out far from the surface. This would reduce corrugation considerably. A surface state of this kind is, however, known to exist on Cu(110) (Ref. 40) and it would again be difficult to explain the difference between Ni and Cu.

(iii) The spillover of electronic charge from the surface into the vacuum is of shorter range for the Sommerfeld model than it is for the jellium model. If this were a true deviation as compared to reality, then the He atom might in our model experience a too strong interaction with the d electrons giving rise to too large corrugation. This, however, should apply for the other metals as well. One has also to bear in mind that the jellium model will definitely overestimate the range of the spillover, because the positive charge is smeared out into the vacuum. Another question is, whether the position of the jellium edge at $d/2$ in front of the first atomic layer is the optimal choice for modeling a realistic surface. Relative small changes in the position of the jellium edge might affect the predicted corrugations significantly. However, no better nonbiased choice is known at present.

(iv) The inward relaxation of the first layer of metal atoms has been neglected in our calculations. This has, however, been estimated by Barker *et al.*[19] to be a small effect having little influence on the corrugation.

(v) Neglect of the corrugation of the sp band. Annett and Haydock[20] propose that this might lead to "anticorrugation" effects. This again should apply to all the metals treated and does not lead to an exceptional result for He/Ni.

As stated before, for He/Ag the repulsive part of the theoretically obtained potential is too steep in comparison to the potential of Schinke and Luntz.[7] This deviation might be attributed to an unrealistic modeling of the silver surface or to the choice of the basis d wave functions.

To check the influence of the d wave functions we compared the He/Ag(110) potentials for adsorption on top of a silver atom using the basis d wave functions described in Table X. These wave functions are usually optimized with the total or orbital energies as criteria or aiming at maximum overlap with Herman-Skillman d wave functions so that they are expected to differ in their degree of accuracy, especially in regions far outside the metal atom, which are in fact important for adsorption of noble-gas atoms. The potential-energy curves for He/Ag(110) using the four different sets of Ag d wave functions are compared in Fig. 17. Obviously the difference in the basis wave functions do not significantly affect the gradient of the repulsive part of the potential. The reasons for the steeper repulsion in the model Hamiltonian results for He/Ag(110) could, however, be tentatively attributed to the following.

TABLE X. Orbital exponents (orb. exp.) and coefficients (coeff.) of Slater-type $4d$ wave functions for different valence states and electron configurations of a silver atom used to calculate the potential-energy curves for He adsorption above Ag(110) in Fig. 17.

	Orb. exp.	Coeff.	Electron configuration	Ref.
A	6.07	0.5889	$Ag^+(d^{10})$	33(c)
	2.663	0.637		
B	4.988 96	0.5798	$Ag^0(d^9s^2)$	33(b)
	2.583 74	0.5756		
C	4.908 14	0.583 30	$Ag^+(d^{10})$	33(d)
	2.444 36	0.580 92		
D	5.704 37	0.321 39	$Ag^+(d^{10})$	33(b)
	3.528 68	0.544 78		
	2.090 46	0.317 97		

In contrast to Ni and Cu the Ag(110) surface does not have an occupied surface state of sp character. This state is shifted above the Fermi level, as has been measured using the method of inverse photoemission.[41] The attractive energy E^{IF} might then be enhanced due to the increased empty charge density. In this case the repulsive part of

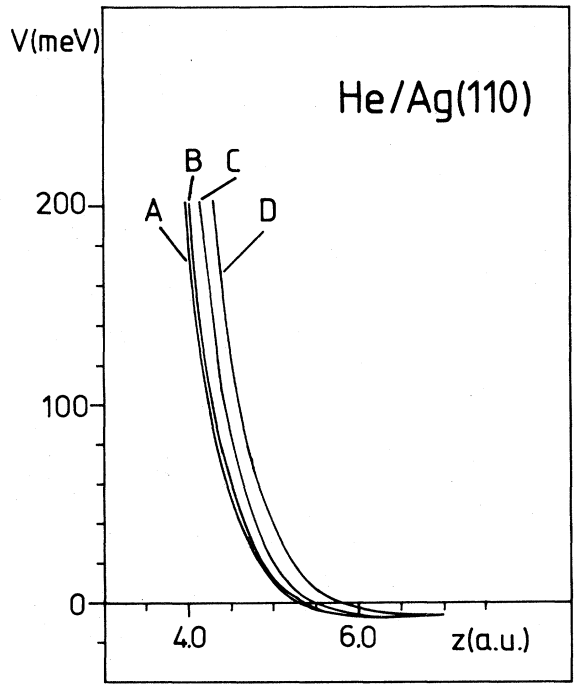

FIG. 17. Potential-energy curves for helium on-top adsorption above Ag(110) using the different basis d wave functions described in Table X.

the potential would be less steep. In a refined treatment surface states obviously have to be considered.

Another possible deficiency of the model—which only becomes important for neon—is the handling of the image potential. As the neon approaches the surface the image corrections to the effective electron-electron repulsion become so large that the two-electron integrals to be used in the Hamiltonian become negative. In the numerical calculations this is prevented by keeping the image-force correction constant from a certain distance, which for neon happens to be near the classical turning points for thermal kinetic energies. Variations of the image correction in the physically reasonable range can therefore easily increase the corrugation by a factor of 1.5. (A decrease is even more unlikely, because our procedure probably underestimates image-force effects.) On the helium atom the electron-electron repulsion is so large that a variation of the image correction within the physical range has practically no effect. This was also checked numerically.

VII. CONCLUSIONS

We have presented potential-energy surfaces for helium and neon interacting with transition metals, obtained by a self-consistent solution of a model Hamiltonian. An improvement about other published approaches is that the *d* electrons are included consistently and nonperturbatively. Interference effects between rare-gas orbitals and metal wave functions as well as image-force effects have been found to be important. The model needs as input a description of the metal surface in the form of one-electron wave functions and their energies. Complete reliable information about clean transition-metal surfaces (including surface states and their wave functions) is not yet available. These uncertainties as well as the rough description of the image force are likely to be responsible for deviations from the experimental data.

ACKNOWLEDGMENTS

D.D. is grateful for the financial support by the Dr. Anton Kalojanoff Stiftung and for the hospitality she encountered in the surface science group of Professor G. Ertl. G.D. acknowledges the support by the Deutsche Forschungsgemeinschaft (Bonn, Germany). This work was also supported by the Sonderforschungsbereich 128, Deutsche Forschungsgemeinschaft. The authors are indebted to Robert Hübner for assistance and discussion.

*Permanent address: Faculty of Chemistry, University of Sofia, Sofia, Bulgaria.

[1]D. V. Tendulkar and R. E. Stickney, Surf. Sci. **27**, 516 (1971); A. G. Stoll and R. P. Merrill, *ibid.* **40**, 405 (1973).

[2]B. F. Mason and B. R. Williams, Surf. Sci. **75**, L786 (1978); J. Lapujoulade, Y. LeCruer, M. Lefort, Y. Lejay, and E. Maurel, *ibid.* **103**, L85 (1981).

[3]J. Lapujoulade, Y. Lejay, and N. Papanicolaou, Surf. Sci. **90**, 133 (1979).

[4]J. Perreau and J. Lapujoulade, Surf. Sci. **119**, L292 (1982); V. B. Salanon, G. Armand, J. Perreau, and J. Lapujoulade, *ibid.* **127**, 135 (1983).

[5]K. H. Rieder and N. Garcia, Phys. Rev. Lett. **49**, 43 (1982).

[6]J. M. Horne and D. R. Miller, Surf. Sci. **66**, 365 (1977).

[7]R. Schinke and A. C. Luntz, Surf. Sci. **124**, L60 (1983).

[8]K. H. Rieder and W. Stocker, Phys. Rev. Lett. **52**, 352 (1984); J. Phys. C **16**, L783 (1983).

[9]K. H. Rieder, T. Engel, R. H. Swendsen, and M. Manninen, Surf. Sci. **127**, 233 (1983).

[10]G. Armand and J. R. Manson, Surf. Sci. **119**, L299 (1982).

[11]J. Harris and A. Liebsch, Phys. Rev. Lett. **49**, 341 (1982); A. Liebsch, J. Harris, B. Salanon, and J. Lapujoulade, Surf. Sci. **123**, 338 (1982).

[12]N. Garcia, J. A. Barker, and I. P. Batra, Solid State Commun. **47**, 485 (1983).

[13]G. G. Kleiman and U. Landman, Phys. Rev. B **8**, 5487 (1973); Phys. Rev. Lett. **31**, 707 (1973); **33**, 524 (1974); Solid State Commun. **18**, 819 (1976).

[14]E. Zaremba and W. Kohn, Phys. Rev. B **13**, 2270 (1976); **15**, 1769 (1977).

[15]V. I. Gerasimenko, Fiz. Tverd. Tela (Leningrad) **19**, 2862 (1977) [Sov. Phys.—Solid State **19**, 1677 (1977)].

[16]J. Harris and A. Liebsch, J. Phys. C **15**, 2275 (1982).

[17]J. E. Van Himbergen and R. Silbey, Solid State Commun. **23**, 623 (1977).

[18]N. D. Lang, Phys. Rev. Lett. **46**, 842 (1981); N. D. Lang and J. K. Nørskov, Phys. Rev. B **27**, 4612 (1982).

[19]J. A. Barker, N. Garcia, I. P. Batra, and M. Baumberger, Surf. Sci. **141**, L317 (1984).

[20]J. F. Annett, R. Haydock, Phys. Rev. Lett. **53**, 838 (1984).

[21]N. Esbjerg and J. K. Nørskov, Phys. Rev. Lett. **45**, 807 (1980).

[22]M. Puska, R. M. Nieminen, and M. Manninen, Phys. Rev. B **24**, 3037 (1981).

[23]B. Salanon, J. Phys. (Paris) **45**, 1373 (1984).

[24]G. Doyen and G. Ertl, J. Chem. Phys. **68**, 5417 (1978).

[25]G. Doyen, Surf. Sci. **59**, 461 (1976).

[26]S. Raimes, *The Wave Mechanics of Electrons in Metals* (North-Holland, Amsterdam, 1963), p. 174.

[27]E. Clementi and D. L. Raimondi, J. Chem. Phys. **38**, 2686 (1963).

[28]J. Hölzl and F. K. Schulte, in *Solid Surface Physics,* Vol. 85 of *Springer Tracts in Modern Physics,* edited by G. Höhler (Springer, Berlin, 1979), p. 1.

[29]L. F. Matheiss, Bull. Am. Phys. Soc., Ser. II **8**, 222 (1963).

[30]F. M. Mueller, A. J. Freeman, J. O. Dimmock, and A. M. Furdyna, Phys. Rev. B **1**, 4617 (1970); N. V. Smith, *ibid.* **9**, 1365 (1974).

[31]J. R. Smith, F. J. Arlinghaus, and J. G. Gay, Phys. Rev. B **22**, 4757 (1980); S. Bhatnagar, Phys. Rev. **183**, 657 (1969).

[32]J. Schmit and A. A. Lucas, Solid State Commun. **11**, 419 (1972).

[33](a) J. W. Richardson, W. C. Nieupoort, R. R. Powell, and W. F. Edgell, J. Chem. Phys. **36**, 1057 (1962); (b) E. Clementi and C. Roetti, At. Data Nucl. Data Tables **14**, 177 (1974); (c) H. Basch and H. B. Gray, Theor. Chim. Acta **4**, 367 (1966); (d) M. Synek and F. Schmitz, Phys. Lett. **27A**, 349 (1968).

[34]W. Sesselmann, Ph.D. thesis, University of Munich, 1983.

[35]J. A. Appelbaum and D. R. Hamann, Phys. Rev. B **6**, 1122 (1972).

[36]G. Doyen and G. Ertl, Surf. Sci. **65**, 641 (1977).

[37]N. Garcia, B. A. Barker, and K. H. Rieder, Solid State Commun. **45**, 567 (1983).

[38]A. Luntz, L. Mattera, M. Rocca, S. Terreni, F. Tommasini, and U. Valbusa, Surf. Sci. **126**, 695 (1983); A. Luntz, L. Mattera, M. Rocca, F. Tommasini, and U. Valbusa, *ibid.* **120**, L447 (1982).

[39]K. Ruedenberg, Rev. Mod. Phys. **34**, 326 (1962).

[40]P. Heimann, J. Hermanson, H. Miosaga, and H. Neddermeyer, Surf. Sci. **85**, 263 (1979).

[41]B. Reihl, R. R. Schlittler, and H. Neff, Phys. Rev. Lett. **52**, 1826 (1984).